ABSTRACT

ARCINIEGA, CRISTINA. Innovative Platforms and Algorithms to Improve Direct Analysis and Mass Spectrometry Imaging (MSI) with Infrared Matrix-Assisted Laser Desorption Electrospray Ionization (IR-MALDESI). (Under the direction of Dr. David C. Muddiman)

Mass spectrometry is a powerful analytical technique that allows the detection and quantification of molecules in a sample. This tool is most commonly used in conjunction with liquid/gas separations. However, the use of mass spectrometry alone for high-throughput screening (HTS) and mass spectrometry imaging (MSI) has been developed in the past decade. IR-MALDESI has been successfully used for both applications. Thus, this dissertation describes the implementation IR-MALDESI for direct analysis from well plates and a novel algorithm for MSI annotations.

The first project describes the construction and coupling of an IR-MALDESI source to a Quadrupole Time-of-Flight (Q-TOF) mass spectrometer for direct analysis from well plates. This project shows the use of a novel IR laser that can fire 1 pulse-per-burst at 100 Hz enabling a quasi-continuous ionization. Additionally, the Q-TOF mass spectrometer continuously analyzes the ions without accumulation. This feature allows the mass spectrometer to have constant resolving power throughout the entire *m/z* range, resulting useful in the analysis of large molecules, such as intact proteins.

Moreover, an extended metal capillary has been developed and tested to extend the inlet of the mass spectrometer. Given that stainless steel has a significantly higher thermal conductivity than glass, we expect the desolvation rate to increase, allowing more ions into the mass spectrometer. The experiments show that the metal capillary woks as well or better than the traditional dielectric glass capillary at introducing ions.

The second project describes a novel database (DB) agnostic of the ionization technique and molecule type for MSI applications. This is a neutral DB and has been developed from MSI

data of various animal and human tissue samples. The DB is customizable by the user allowing the addition of new molecules detected. Furthermore, a novel searching algorithm is presented to annotate MSI data. This algorithm supports multiply-charged species by allowing the user to select the desired adducts to search the DB. The adducts list is also customizable by the user.

An MSI workflow using MSiReader is presented to pre-process data, create a list of ions, and annotate data. An example is shown to annotate *N*-linked glycans. This example shows the use of tools to centroid profile data, select an abundance threshold, perform mass correction, determine “on-tissue” ions, and annotate data.

Innovative Platforms and Algorithms to Improve Direct Analysis and Mass Spectrometry Imaging (MSI) with Infrared Matrix-Assisted Laser Desorption Electrospray Ionization (IR-MALDESI)

by

Cristina Arciniega

A dissertation submitted to the Graduate Faculty of

North Carolina State University

in partial fulfilment of the

requirements for the degree of

Master of Science

Chemistry

Raleigh, North Carolina,

2023

APPROVED BY:

David C. Muddiman	Yi Xiao
Chair of Advisory Committee	

Reza A. Ghiladi

DEDICATION

To Esperanza, you gave me the hope I needed to keep going during the hardest times.

BIOGRAPHY

Cristina Arciniega was born and raised in Quito – Ecuador. During her high-school studies she developed a passion for math and chemistry. She was awarded a national scholarship that allowed her to pursue an undergraduate degree in any university throughout Ecuador. In this way, she completed her undergraduate studies in Chemical Engineering at Universidad San Francisco de Quito. During her undergraduate thesis, Cristina worked doing research in fast pyrolysis of cellulose. To analyze the products, she used gas chromatography (GC) and gas chromatography coupled to mass spectrometry (GC-MS), where she realized had a passion for analytical chemistry and a desire to learn more about mass spectrometry. After graduation, Cristina collaborated at the same university as a Laboratory instructor, where she found great joy on training and helping students on their learning journey.

Cristina moved to Raleigh, North Carolina and started her work towards a master's degree in Analytical Chemistry at NC State University under the supervision of Dr. David Muddiman. She has developed new skills and learned analytical techniques through her research and teaching assignments. Cristina has taught two advanced analytical laboratory courses. Her first research project was a collaboration with Agilent Technologies which allowed her to do an internship in California. After this experience, Cristina is eager to find an industrial career that will allow her to develop new solutions using mass spectrometry and analytical chemistry. She currently resides in Raleigh with her husband Julio and their cat Benito.

ACKNOWLEDGEMENTS

I'd like to extend the most grateful acknowledgement to Dave Muddiman for being a great mentor and an amazing advisor. Thank you for your guidance and for showing me the wonderful things we can do with mass spectrometry. Before joining NC State, I barely had any knowledge of this technique and, in this research group, I have learned and grown so much. Thank you for being an amazing person who cares about people first over anything else. I appreciate your advice, not only the professional but the personal guidance you have given me. Thank you for taking the time to watch your students grow and for teaching us to be independent scientists. I have learned so many things from you, which I hope I can replicate in my life as well.

I would also like to thank Ken Garrard for being such an amazing person who has made an impact in my life. I love how kind you are, always willing to help and to teach. I am continuously amazed by your knowledge and experience, and I am grateful you shared it with me. Thank you for helping me with my research project, even when I was in California with a 3-hour difference. I am so glad I got to collaborate and learn from you.

I would also like to thank all the members of the Muddiman Lab. You are all amazing people and great scientists. I admire your work and your enthusiasm to pursue science. Thank you for your support and for the great experiences we have had together. I wish you all the best in your lives and your careers and I look forward to the amazing things you will do in the field.

I want to thank Agilent Technologies for the funding and the collaboration. I'd like to specially thank Alex Apffel for being a great person, introducing me to amazing people (including your wife Julie), and for mentoring me during my time in California, I learned a lot from you. I'd also like to thank Laurakay Bruhn, Trygve Ristroph, Reid (Turtle) Brennen, and Hannah Cheung.

To my parents, thank you for your continuous support. I am grateful to have you in my life. Thank you for pushing me to be better every day. I love you and I hope I show you with my actions how much I do.

I want to give special thanks to my wonderful husband Julio. Thank you for being my support during the good and bad times, especially the bad ones. I am so happy to have you in my life and to be able to share my experiences with you. Thank you for lifting me up in the worst times and for always taking care of me. I love you and I am grateful to have you in my life.

Finally, I'd like to thank myself for being an enthusiastic person who's always trying to find something good out of things. I am happy to finish this degree and ready to pursue new challenges. I wouldn't want to be anyone else, but me 😊

TABLE OF CONTENTS

LIST OF TABLES

LIST OF FIGURES

Chapter 1 Introduction to Mass Spectrometry

Mass spectrometry is one of the most powerful and indispensable analytical tools nowadays. It is widely employed in different scientific fields due to its high sensitivity, selectivity, accuracy, and high throughput capabilities.[1] This technique relies on the formation of gas-phase ions, which can be positively or negatively charged, to analyze the molecular composition of a sample.[2] MS allows the study of molecules by measuring and separating the ions according to their mass-to-charge ratio (*m*/z). Consequently, a mass spectrum is the plot of ion abundance vs. *m/z*.[3]

Different types of mass spectrometers exist in the market; nevertheless, all of them contain three main parts: the ionization source, a mass analyzer, and a detector as shown in **Figure 1.1**. The selection of each of these parts should be based on the sample type and analyte(s) of interest being studied. The choice can substantially alter the qualitative and quantitative data obtained. Especially relevant to the work presented here are the ionization sources and mass analyzers used, for which a detailed explanation is presented.

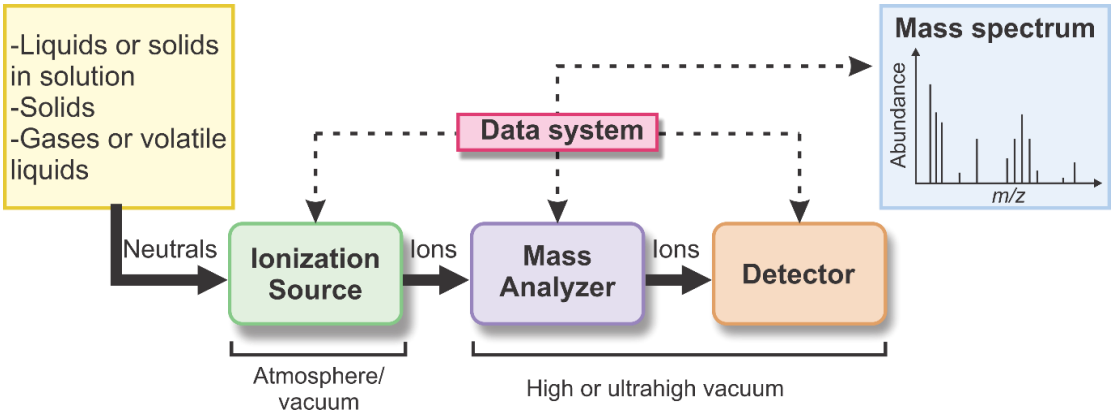

Figure 1.1. General layout of mass spectrometers. The ionization sources operate at atmospheric pressure or vacuum, depending on the technique. The data system collects the abundance of all the ions detected and creates the mass spectrum.

1.1 Ionization Sources

The ionization source introduces a sample into the mass spectrometer. This process transforms a solid, liquid, or gas sample into gas-phase ions either thermally, with electric fields, or by impacting energetic electrons, ions, or photons[4]. There are many types of ionization techniques used for different applications and samples. They can be roughly classified by their relative hardness or softness, regarding the molecular preservation, and molecular mass of analytes, as shown in **Figure 1.2**. An ionization method is considered soft when it is able to produce intact ions from molecular species without fragmentation[5]. Moreover, the ion generation process can be performed in a vacuum or at atmospheric pressure.

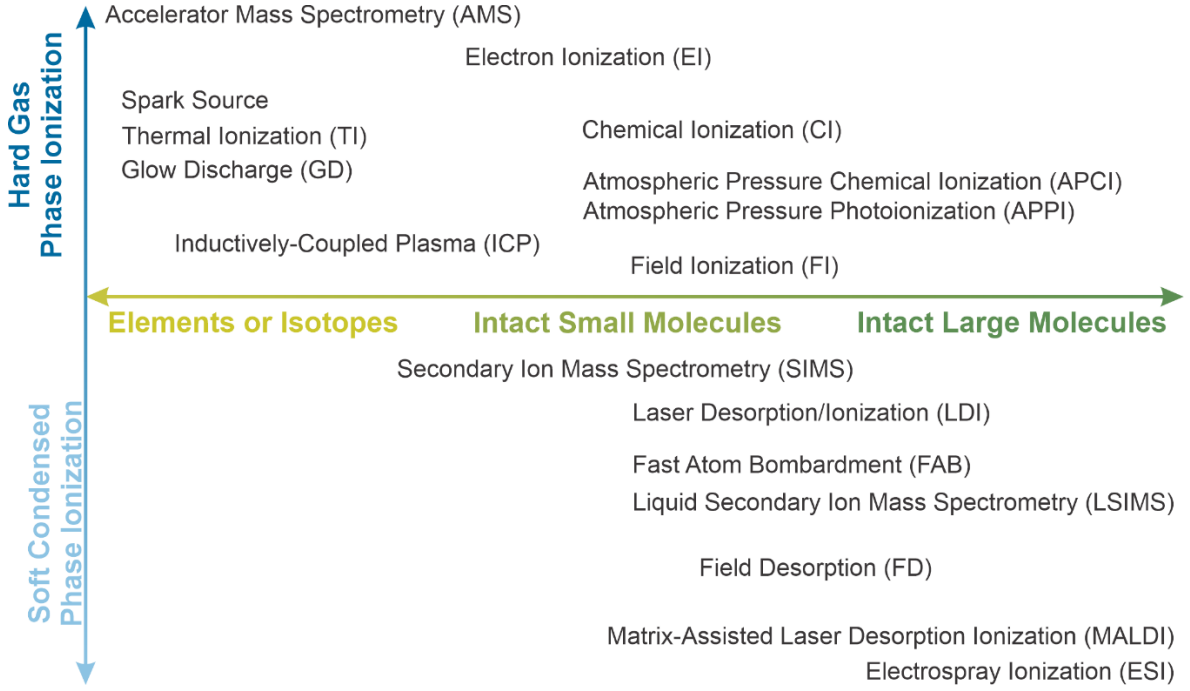

Figure 1.2 Ionization techniques classified by their analyte of interest and their relative hardness/softness. Figure adapted from Gross, J.[4]

Electrospray ionization (ESI) and Matrix-Assisted Laser Desorption Ionization (MALDI) have become the most popular techniques due to their softness and their application to biological samples[6–8]. Infrared Matrix-Assisted Laser Desorption Electrospray Ionization (IR-MALDESI) is a hybrid ionization technique that uses both principles of MALDI and ESI. Given their relevance to

the invention of IR-MALDESI, a detailed explanation of these techniques and their ionization mechanism is given below.

1.1.1 Electrospray Ionization (ESI)

ESI is an atmospheric pressure technique, and it is considered the softest ionization source for mass spectrometry. It allows the direct coupling of liquid separations (*i.e.,* liquid chromatography (LC)) to a mass spectrometer (*i.e.,* LC-MS)[9] through the ionization of the liquid phase from the separation column. LC-MS and ESI enhanced the use of mass spectrometry in the analysis of biological samples. LC helps with the separation of complex mixtures whilst ESI provides the capability to generate multiply-charged molecules with multiple basic sites in positive polarity (the equivalent for negative polarity)[9] (*e.g.,* proteins) and non-covalent complexes. The capability to multiply charge molecules allows the detection of these analytes in a lower *m/z* range, allowing the use of high-resolving power instruments, such as Fourier Transform Ion Cyclotron Resonance (FT-ICR) and Orbitrap-based mass spectrometers.

ESI consists of applying a high voltage (2-5 kV) between the capillary emitter tip and the inlet to the mass spectrometer as shown in **Figure 1.3**. The diluted sample flows through the emitter tip at low flow rates (1-20 μL/min). When it reaches the tip of the capillary needle, the charge accumulates allowing the formation of a Taylor cone[10] and a plume of ions. The charged droplets in the plume are reduced in size due to desolvation. When the charge exceeds the Rayleigh limit the precursor droplets undergo the Columbic fission **Eq. (1)** to form progeny droplets of smaller size.

$$q_r = 8\pi(\gamma\varepsilon_0)^{1/2}r^{3/2} \quad \textbf{(1)}$$

Where q_r is the charge of the droplet [C], ε_0 is the permittivity of free space [F/m], γ is the surface tension of the droplet [N/m], $\boldsymbol{r}$ is the droplet's radius [m].

There are two proposed mechanisms of ionization for electrospray: the charge residue model (CRM), and the ion evaporation model (IEM). The scientific community still debates which mechanism governs the ionization process. However, it is generally believed that IEM applies for small molecules and CRM for large molecules. **Figure 1.3** shows a schematic of both ionization mechanisms. In both cases, the progeny droplet undergoes Coulombic fission and generates offspring droplets. The difference between both mechanisms relies on the formation of gas-phase ions from the offspring droplets.

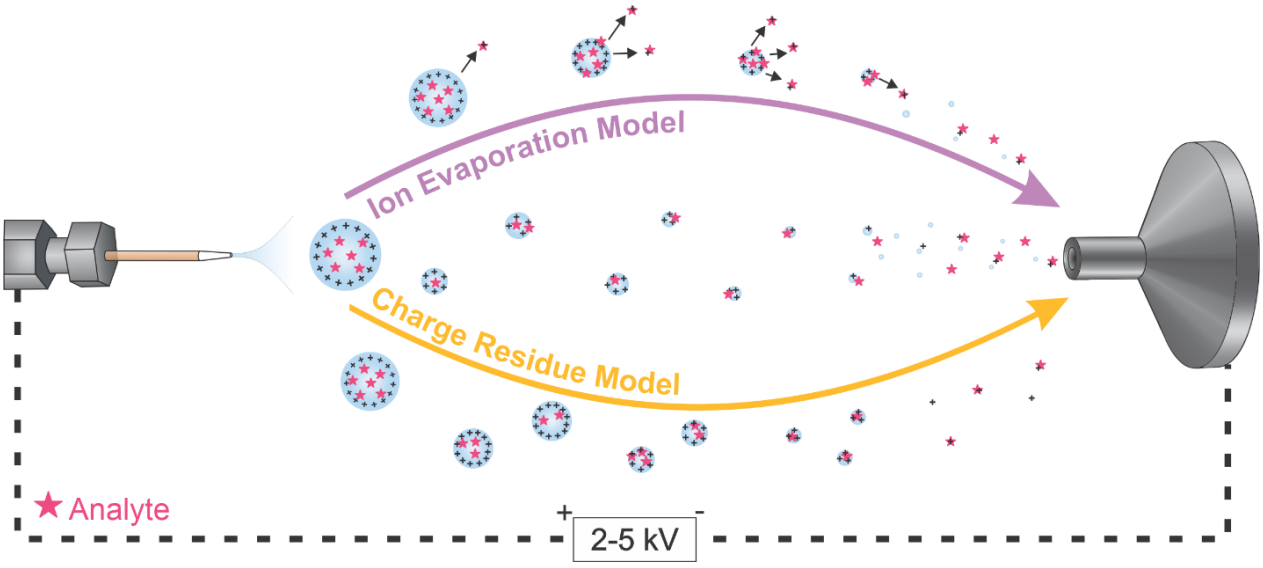

Figure 1.3. Schematic representation of electrospray ionization (ESI) mechanisms. In purple, the Ion Evaporation Model (IEM) shows the analyte is being ejected from the droplet with one or multiple charges. In yellow, the Charge Residue Model (CRM) shows the droplets partition into smaller droplets until the solvent completely evaporates and the analyte is charged.

The CRM considers that the larger droplets are repeatedly partitioned into offspring droplets until the solvent completely evaporates, transferring the charges to the molecule inside[11,12]. This theory applies to large molecules (MDa sized) given that it has been observed that one offspring droplet can only contain one molecule of that size[13]. Thus, after solvent evaporation is complete, the only molecule present will be able to hold all of the charges from the droplet. Nevertheless, this model does not explain the selectivity of ion formation from mixtures.

The IEM, on the other hand, considers that the molecules are ejected with a charge from the offspring droplet before it undergoes Columbic fission. As the solvent evaporates and the droplet gets smaller the molecules closer to the surface are emitted directly with multiple charges[14–17]. The number of charges a molecule can take depends on various things: the number of available sites for protonation or deprotonation, the geometry of the molecule, its hydrophobicity, and the number of charges the droplet carries[18]. Hydrophilic molecules are highly solvated and will be situated in the middle of the droplet. Hydrophobic molecules, alternatively, will be closer to the surface of the droplet due to their high surface activity. These molecules are more likely to have high charge-to-mass ratios given that they easily partition into offspring droplets and can be desorbed directly from the surface acquiring multiple charges[19,20].

1.1.1. Matrix-Assisted Laser Desorption Ionization (MALDI)

Laser desorption ionization (LDI) techniques have been used in mass spectrometry since the 1960s[21,22]. However, the use of a matrix has been proven to aid the desorption/ionization event, allowing the analysis of diverse samples while also increasing the ion abundance[23]. The matrix and the laser wavelength must go in hand, allowing the laser to excite and desorb the sample[24]. MALDI has been proven to be a soft ionization technique, with low limits of detection, by analyzing large molecules (*i.e.,* proteins) without fragmentation[25,26]. Due to its softness, it has been widely employed in the analysis of biological samples.

The current workflow for sample preparation for MALDI analysis consists of mixing the analyte with the matrix and further crystallization. The matrix to analyte molar ratio should be *ca.* 2000:1 to allow for an excess of matrix to absorb the laser's energy. It is preferred to have a fast evaporation that yields microcrystals since large crystals decrease shot-to-shot reproducibility. After firing the laser, the matrix and analyte are desorbed causing the microcrystals to be sublimated into the gas phase. MALDI mass spectra typically show singly-charged species, which are spread in the *m/z* range making interpretation straightforward.

The role of the matrix is to absorb laser energy, become ionized, and provide a source of protons to charge the analyte. MALDI experiments typically use an organic matrix that absorbs energy in the UV range, and a UV laser. Choosing the matrix depends on the analyte of interest. Highly polar analytes work well with highly polar matrices. Matrix-analyte solutions are typically in an acid/organic mixture with a pH less than 4. Two mechanisms explain the ionization process of MALDI, the "Lucky Survivor" theory and Gas Phase ionization[27]. **Figure 1.4** shows schemes of both ionization processes. Each of these mechanisms has been demonstrated[28] and they both take place in the analyte's ion formation.

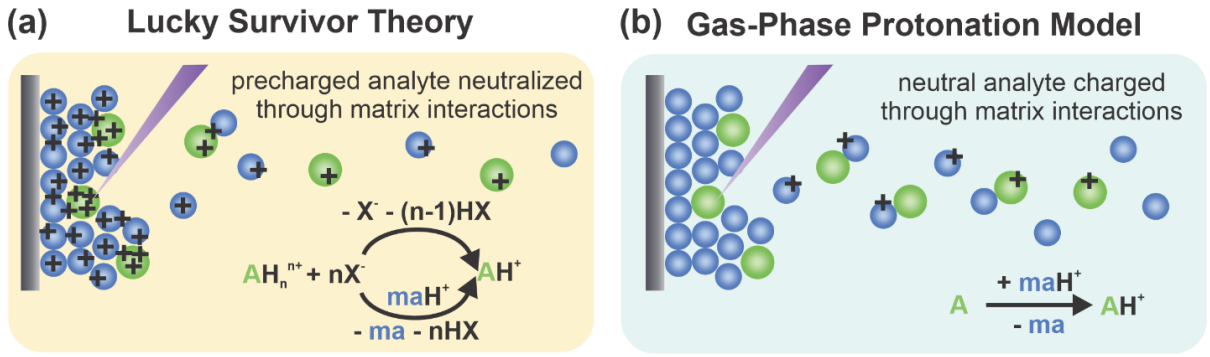

Figure 1.4. Scheme of the MALDI ionization mechanisms **(a)** "Lucky Survivor" Theory and **(b)** Gas-phase protonation model.

The lucky survivor theory states that a molecule that was charged in solution will stay charged after co-crystallization with the matrix. Since the matrix-analyte mixture typically occurs at low pHs, a slightly basic analyte will be protonated in solution. Therefore, when the laser fires and desorbs the sample, the matrix ions neutralize the charges of the protonated analyte in the gas phase, until only one charge remains. See **Figure 1.4 (a)**.

The gas-phase protonation model, on the other hand, states that the matrix absorbs energy from the laser, generates and transfers protons to the analyte while in the gas phase. The matrix ions and the neutral molecules of the analyte undergo collision events in which the charge is transferred. The analyte should have a negative enthalpy of reaction or a higher affinity to the charge for it to be ionized by the matrix intreractions[29] . See **Figure 1.4 (b)**.

1.1.2. Matrix-Assisted Laser Desorption Electrospray Ionization (MALDESI)

This ionization technique was first introduced by Sampson, *et. al.*, for the analysis of polypeptides[30]. MALDESI is a hybrid ionization technique that combines matrix-assisted laser desorption with electrospray ionization[31]. While UV laser was first used at its inception, an infrared laser has been more commonly applied for a wide range of biological studies. This ionization source uses an infrared (IR) laser which operates at 2.97 µm. The IR laser does not provide sufficient energy to ionize the sample, therefore the plume of neutrals desorbed from the sample and are further ionized by the orthogonal ESI plume, making this a soft ionization technique comparable to ESI. The IR wavelength resonantly excites the O-H stretching bands; thus water/ice can be used as a matrix to enhance the desorption event. However, the matrix does not contribute to the ionization process, unlike with MALDI[32]. This ionization technique has been widely used for Mass Spectrometry Imaging (MSI) of metabolites[33–35], *N*-glycans[36], plants[37], single-cell analyses[38], 3D imaging[39], and direct analysis[40–42]. Previously this source has been coupled to FT-ICR and Orbitrap-based mass spectrometers due to their high resolution and accurate mass capabilities.

1.2 Mass Analyzers

The gas-phase ions generated by the ionization source enter the mass spectrometer and are separated by their mass-to-charge ratio (*m/z*) in the mass analyzer. There are a variety of mass analyzers in the market for different applications such as targeted and untargeted studies. Mass analyzers can be divided into two groups: pulsed and scanning. Pulsed mass analyzers provide simultaneous detection of all ions; examples are Time-of-Flight (TOF), Fourier Transform Ion Cyclotron Resonance (FT-ICR), and Orbitrap. Scanning mass analyzers, on the other hand, provide the detection of different *m/z* values successively along a time scale; examples are Linear Quadrupole, Quadrupole Ion Trap (QIT), and Magnetic Sector. This work focuses on coupling IR-

MALDESI to a Quadrupole Time-of-Flight (Q-TOF), therefore a detailed explanation of the TOF mass analyzer is presented.

1.2.1 Time of Flight (TOF)

The Time-of-Flight mass analyzer was first introduced in the 1950s[43,44]. The principle consists of measuring the transient time ions of different *m/z* are required to travel a field-free drift path of fixed length. Unfortunately, the lack of technologies to facilitate the processing and recording of data in the microsecond timeframe caused TOF instruments to have issues associated with limited resolving power, detection, sensitivity, and signal problems[45]. Hence, the use of TOF instruments was displaced by magnetic and quadrupole instruments with higher sensitivity and resolving power.

In a TOF mass analyzer, ions receive a similar amount of kinetic energy during an acceleration process. The velocities are different due to their masses; thus, ions of different *m/z* arrive at different times to the detector. After performing an energy balance considering the kinetic and potential energies for a particular ion traveling through the mass analyzer, we obtain **Eq. (2)**, which shows the relationship between *m/z* and the velocity of the ion. The traveling time of an ion through a fixed length s of field-free space is given by **Eq (3)**.

$$\frac{m}{z} = \frac{2eU}{bv^2} \quad \textbf{(2)}$$

$$t = s\sqrt{\frac{bm}{2zeU}} \quad \textbf{(3)}$$

Where m is the monoisotopic mass of a chemical species [Da], z elemental charge of the ion, e elemental charge of an electron (1.6022x10^{-19} [C]), U acceleration voltage [V], b conversion factor from Da to kg (1.6605x10^{-27} [kg/Da]), v velocity of the ion [m/s], t traveling time [s], and s traveling distance [m].

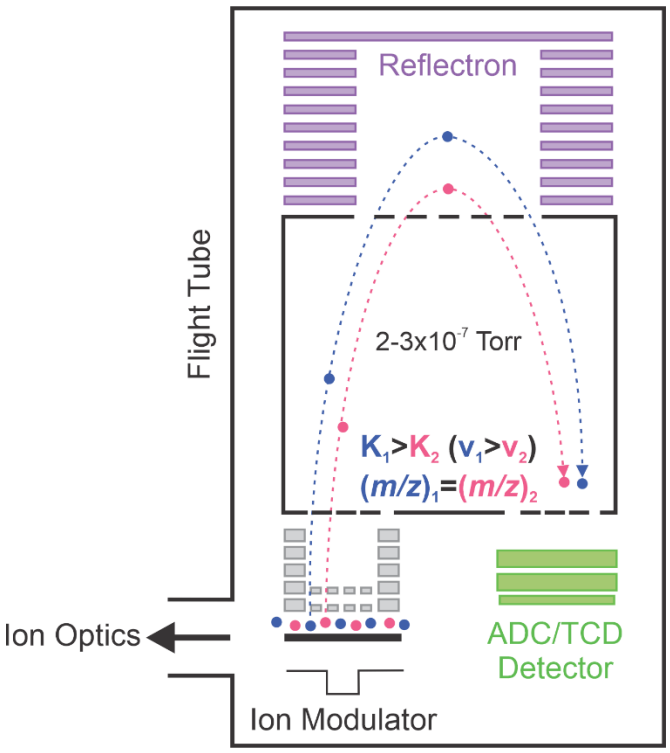

Figure 1.5. Schematic representation of a Time-of-Flight (TOF) mass analyzer. The ion modulator pulses the ions with a voltage towards the flight path. The ions reach the reflectron and are bounced back towards the detector. The reflectron corrects the differences in kinetic energy for two ions of the same *m/z*. Adapted from Chernusevich et al. and Guilhaus[46,47]

The development of MALDI sources in the late 1980s brought back the use of TOF instruments due to their need of a pulsed mass analyzer. New technologies allowed the development of reflectrons[48], discrete detectors, and acquisition methods which increased the resolution and solved the previous mentioned problems. The reflectron serves as an ion mirror, correcting the kinetic energy differences and allowing the flight path to be doubled. A schematic representation of an orthogonal TOF mass analyzer with a reflectron is shown in **Figure 1.5**. Nowadays, TOF analyzers have been adapted for use with multiple ionization sources (*e.g.,* ESI, APCI) and have become widely used along with FT-ICR and Orbitrap instruments[49,50].

1.3 Research synopsis

This thesis describes the development and applications of IR-MALDESI in the field of mass spectrometry. IR-MALDESI coupled to an Orbitrap mass spectrometer has previously been

used for high throughput screening applications. Nonetheless, the acquisition speed of an Orbitrap mass analyzer is highly dependent on the resolving power (*i.e.,* lower resolving power allows for higher throughput). On the other hand, for a Quadrupole Time-of Flight (Q-TOF) the resolving power is constant and not limited by the acquisition speed. Consequently, **Chapter 2** presents the coupling of IR-MALDESI to an Agilent Q-TOF for direct analysis from well plates. This work shows a proof of concept for high throughput screening applications using a Q-TOF mass spectrometer.

Additionally, mass spectrometry imaging (MSI) is a field that has been developed during the last decade. This technique has shown promising results in the study of diseases by spatially resolving molecular information. Nevertheless, the databases (DBs) used for MSI annotations have been elaborated based on liquid chromatography-tandem mass spectrometry (LC-MS/MS) data. The need for an MSI centered DB is of great importance in the field. Henceforth, **Chapter 3** presents the development of a database for mass spectrometry imaging (MSI) annotations and demonstrates a detailed MSI workflow to annotate data using the novel DB.

1.4 References

(1) Awad, H.; Khamis, M. M.; El-Aneed, A. Mass Spectrometry, Review of the Basics: Ionization. *Appl Spectrosc Rev* **2015**, *50* (2), 158–175. https://doi.org/10.1080/05704928.2014.954046.

(2) El-Aneed, A.; Cohen, A.; Banoub, J. Mass Spectrometry, Review of the Basics: Electrospray, MALDI, and Commonly Used Mass Analyzers. *Appl Spectrosc Rev* **2009**, *44* (3), 210–230. https://doi.org/10.1080/05704920902717872.

(3) Glish, G. L.; Vachet, R. W. The Basics of Mass Spectrometry in the Twenty-First Century. *Nat Rev Drug Discov* **2003**, *2* (2), 140–150. https://doi.org/10.1038/nrd1011.

(4) Gross, J. H. *Mass Spectrometry*, 3rd ed.; Springer International Publishing, 2017. https://doi.org/10.1007/978-3-319-54398-7.

(5) Fenn, J. B.; Mann, M.; Meng, C. K.; Wong, S. F.; Whitehouse, C. M. Electrospray Ionization for Mass Spectrometry of Large Biomolecules. *Science (1979)* **1989**, *246* (4926), 64–71. https://doi.org/10.1126/science.2675315.

(6) Cole, R. B. *Electrospray and MALDI Mass Spectrometry*; John Wiley & Sons, Inc.: Hoboken, NJ, USA, 2010. https://doi.org/10.1002/9780470588901.

(7) Chapman, J. R. *Mass Spectrometry of Proteins and Peptides*; Humana Press: New Jersey, 2000; Vol. 146. https://doi.org/10.1385/1592590454.

(8) Siuzdak, G. The Expanding Role of Mass Spectrometry in Biotechnology. *J Am Soc Mass Spectrom* **2004**, *15* (4), 625–625. https://doi.org/10.1016/j.jasms.2003.12.009.

(9) Abian, J. The Coupling of Gas and Liquid Chromatography with Mass Spectrometry. *Journal of Mass Spectrometry* **1999**, *34* (3), 157–168. https://doi.org/10.1002/(SICI)1096-9888(199903)34:3<157::AID-JMS804>3.0.CO;2-4.

(10) Taylor, G. I. Disintegration of Water Drops in an Electric Field. *Proc R Soc Lond A Math Phys Sci* **1964**, *280* (1382), 383–397. https://doi.org/10.1098/rspa.1964.0151.

(11) Dole, M.; Mack, L. L.; Hines, R. L.; Chemistry, D. O.; Mobley, R. C.; Ferguson, L. D.; Alice, M. B. Molecular Beams of Macroions. *J Chem Phys* **1968**, *49* (5), 2240–2249. https://doi.org/10.1063/1.1670391.

(12) Kebarle, P.; Peschke, M. On the Mechanisms by Which the Charged Droplets Produced by Electrospray Lead to Gas Phase Ions. *Anal Chim Acta* **2000**, *406* (1), 11–35. https://doi.org/10.1016/S0003-2670(99)00598-X.

(13) Wilm, M. S.; Mann, M. Electrospray and Taylor-Cone Theory, Dole's Beam of Macromolecules at Last? *Int J Mass Spectrom Ion Process* **1994**, *136* (2–3), 167–180. https://doi.org/10.1016/0168-1176(94)04024-9.

(14) Iribarne, J. V. On the Evaporation of Small Ions from Charged Droplets. *J Chem Phys* **1976**, *64* (6), 2287. https://doi.org/10.1063/1.432536.

(15) Thomson, B. A.; Iribarne, J. V. Field Induced Ion Evaporation from Liquid Surfaces at Atmospheric Pressure. *J Chem Phys* **1979**, *71* (11), 4451–4463. https://doi.org/10.1063/1.438198.

(16) Nguyen, S.; Fenn, J. B. Gas-Phase Ions of Solute Species from Charged Droplets of Solutions. *Proceedings of the National Academy of Sciences* **2007**, *104* (4), 1111–1117. https://doi.org/10.1073/pnas.0609969104.

(17) Yamashita, M.; Fenn, J. B. Electrospray Ion Source. Another Variation on the Free-Jet Theme. *J Phys Chem* **1984**, *88* (20), 4451–4459. https://doi.org/10.1021/j150664a002.

(18) Fenn, J. B. Ion Formation from Charged Droplets: Roles of Geometry, Energy, and Time. *J Am Soc Mass Spectrom* **1993**, *4* (7), 524–535. https://doi.org/10.1016/1044-0305(93)85014-O.

(19) Cech, N. B.; Enke, C. G. Practical Implications of Some Recent Studies in Electrospray Ionization Fundamentals. *Mass Spectrom Rev* **2001**, *20* (6), 362–387. https://doi.org/10.1002/mas.10008.

(20) Null, A. P.; Nepomuceno, A. I.; Muddiman, D. C. Implications of Hydrophobicity and Free Energy of Solvation for Characterization of Nucleic Acids by Electrospray Ionization Mass Spectrometry. *Anal Chem* **2003**, *75* (6), 1331–1339. https://doi.org/10.1021/ac026217o.

(21) Fenner, N. C.; Daly, N. R. Laser Used for Mass Analysis. *Review of Scientific Instruments* **1966**, *37* (8), 1068–1070. https://doi.org/10.1063/1.1720410.

(22) Vastola, F. J.; Mumma, R. O.; Pirone, A. J. Analysis of Organic Salts by Laser Ionization. *Organic Mass Spectrometry* **1970**, *3* (1), 101–104. https://doi.org/10.1002/oms.1210030112.

(23) Karas, M.; Bachmann, D.; Bahr, U.; Hillenkamp, F. Matrix-Assisted Ultraviolet Laser Desorption of Non-Volatile Compounds. *Int J Mass Spectrom Ion Process* **1987**, *78*, 53–68. https://doi.org/10.1016/0168-1176(87)87041-6.

(24) Karas, Michael.; Bachmann, Doris.; Hillenkamp, Franz. Influence of the Wavelength in High-Irradiance Ultraviolet Laser Desorption Mass Spectrometry of Organic Molecules. *Anal Chem* **1985**, *57* (14), 2935–2939. https://doi.org/10.1021/ac00291a042.

(25) Karas, M.; Ingendoh, A.; Bahr, U.; Hillenkamp, F. Ultraviolet-Laser Desorption/Ionization Mass Spectrometry of Femtomolar Amounts of Large Proteins. *Biol Mass Spectrom* **1989**, *18* (9), 841–843. https://doi.org/10.1002/bms.1200180931.

(26) Karas, Michael.; Hillenkamp, Franz. Laser Desorption Ionization of Proteins with Molecular Masses Exceeding 10,000 Daltons. *Anal Chem* **1988**, *60* (20), 2299–2301. https://doi.org/10.1021/ac00171a028.

(27) Karas, M.; Glückmann, M.; Schäfer, J. Ionization in Matrix-Assisted Laser Desorption/Ionization: Singly Charged Molecular Ions Are the Lucky Survivors. *Journal of Mass Spectrometry* **2000**, *35* (1), 1–12. https://doi.org/10.1002/(SICI)1096-9888(200001)35:1<1::AID-JMS904>3.0.CO;2-0.

(28) Jaskolla, T. W.; Karas, M. Compelling Evidence for Lucky Survivor and Gas Phase Protonation: The Unified MALDI Analyte Protonation Mechanism. *J Am Soc Mass Spectrom* **2011**, *22* (6), 976–988. https://doi.org/10.1007/s13361-011-0093-0.

(29) Zenobi, R.; Knochenmuss, R. Ion Formation in MALDI Mass Spectrometry. *Mass Spectrom Rev* **1998**, *17* (5), 337–366. https://doi.org/10.1002/(SICI)1098-2787(1998)17:5<337::AID-MAS2>3.0.CO;2-S.

(30) Sampson, J. S.; Hawkridge, A. M.; Muddiman, D. C. Generation and Detection of Multiply-Charged Peptides and Proteins by Matrix-Assisted Laser Desorption Electrospray Ionization (MALDESI) Fourier Transform Ion Cyclotron Resonance Mass Spectrometry. *J Am Soc Mass Spectrom* **2006**, *17* (12), 1712–1716. https://doi.org/10.1016/j.jasms.2006.08.003.

(31) Caleb Bagley, M.; Garrard, K. P.; Muddiman, D. C. The Development and Application of Matrix Assisted Laser Desorption Electrospray Ionization: The Teenage Years. *Mass Spectrom Rev* **2021**, mas.21696. https://doi.org/10.1002/mas.21696.

(32) Dixon, R. B.; Muddiman, D. C. Study of the Ionization Mechanism in Hybrid Laser Based Desorption Techniques. *Analyst* **2010**, *135* (5), 880. https://doi.org/10.1039/b926422a.

(33) Sohn, A. L.; Ping, L.; Glass, J. D.; Seyfried, N. T.; Hector, E. C.; Muddiman, D. C. Interrogating the Metabolomic Profile of Amyotrophic Lateral Sclerosis in the Post-Mortem Human Brain by Infrared Matrix-Assisted Laser Desorption Electrospray Ionization (IR-MALDESI) Mass Spectrometry Imaging (MSI). *Metabolites* **2022**, *12* (11), 1096. https://doi.org/10.3390/metabo12111096.

(34) Mellinger, A. L.; Garrard, K. P.; Khodjaniyazova, S.; Rabbani, Z. N.; Gamcsik, M. P.; Muddiman, D. C. Multiple Infusion Start Time Mass Spectrometry Imaging of Dynamic SIL-Glutathione Biosynthesis Using Infrared Matrix-Assisted Laser Desorption Electrospray Ionization. *J Proteome Res* **2022**, *21* (3), 747–757. https://doi.org/10.1021/acs.jproteome.1c00636.

(35) Pace, C. L.; Horman, B.; Patisaul, H.; Muddiman, D. C. Analysis of Neurotransmitters in Rat Placenta Exposed to Flame Retardants Using IR-MALDESI Mass Spectrometry Imaging. *Anal Bioanal Chem* **2020**, *412* (15), 3745–3752. https://doi.org/10.1007/s00216-020-02626-4.

(36) Pace, C. L.; Angel, P. M.; Drake, R. R.; Muddiman, D. C. Mass Spectrometry Imaging of *N* -Linked Glycans in a Formalin-Fixed Paraffin-Embedded Human Prostate by Infrared Matrix-Assisted Laser Desorption Electrospray Ionization. *J Proteome Res* **2022**, *21* (1), 243–249. https://doi.org/10.1021/acs.jproteome.1c00822.

(37) Bagley, M. C.; Pace, C. L.; Ekelöf, M.; Muddiman, D. C. Infrared Matrix-Assisted Laser Desorption Electrospray Ionization (IR-MALDESI) Mass Spectrometry Imaging Analysis of Endogenous Metabolites in Cherry Tomatoes. *Analyst* **2020**, *145* (16), 5516–5523. https://doi.org/10.1039/D0AN00818D.

(38) Xi, Y.; Tu, A.; Muddiman, D. C. Lipidomic Profiling of Single Mammalian Cells by Infrared Matrix-Assisted Laser Desorption Electrospray Ionization (IR-MALDESI). *Anal Bioanal Chem* **2020**, *412* (29), 8211–8222. https://doi.org/10.1007/s00216-020-02961-6.

(39) Bai, H.; Khodjaniyazova, S.; Garrard, K. P.; Muddiman, D. C. Three-Dimensional Imaging with Infrared Matrix-Assisted Laser Desorption Electrospray Ionization Mass Spectrometry. *J Am Soc Mass Spectrom* **2020**, *31* (2), 292–297. https://doi.org/10.1021/jasms.9b00066.

(40) Pace, C. L.; Muddiman, D. C. Direct Analysis of Native *N* -Linked Glycans by IR-MALDESI. *J Am Soc Mass Spectrom* **2020**, *31* (8), 1759–1762. https://doi.org/10.1021/jasms.0c00176.

(41) Knizner, K. T.; Bagley, M. C.; Garrard, K. P.; Hauschild, J.-P.; Pu, F.; Elsen, N. L.; Williams, J. D.; Muddiman, D. C. Optimized C-Trap Timing of an Orbitrap 240 Mass Spectrometer

for High-Throughput Screening and Native MS by IR-MALDESI. *J Am Soc Mass Spectrom* **2022**, *33* (2), 328–334. https://doi.org/10.1021/jasms.1c00319.

(42) Knizner, K. T.; Bagley, M. C.; Pu, F.; Elsen, N. L.; Williams, J. D.; Muddiman, D. C. Normalization Techniques for High-throughput Screening by Infrared Matrix-assisted Laser Desorption Electrospray Ionization Mass Spectrometry. *Journal of Mass Spectrometry* **2022**, *57* (6). https://doi.org/10.1002/jms.4869.

(43) Stephens, W. E. A Pulsed Mass Spectrometer with Time Dispersion. *Physical Review* **1946**, *69*, 691.

(44) Wolff, M. M.; Stephens, W. E. A Pulsed Mass Spectrometer with Time Dispersion. *Review of Scientific Instruments* **1953**, *24* (8), 616–617. https://doi.org/10.1063/1.1770801.

(45) Guilhaus, M. Special Feature: Tutorial. Principles and Instrumentation in Time-of-Flight Mass Spectrometry. Physical and Instrumental Concepts. *Journal of Mass Spectrometry* **1995**, *30* (11), 1519–1532. https://doi.org/10.1002/jms.1190301102.

(46) Chernushevich, I. V.; Loboda, A. V.; Thomson, B. A. An Introduction to Quadrupole-Time-of-Flight Mass Spectrometry. *Journal of Mass Spectrometry* **2001**, *36* (8), 849–865. https://doi.org/10.1002/jms.207.

(47) Guilhaus, M. MASS SPECTROMETRY | Time-of-Flight. In *Encyclopedia of Analytical Science*; Elsevier, 2005; pp 412–423. https://doi.org/10.1016/B0-12-369397-7/00347-2.

(48) Mamyrin, B. A. Laser Assisted Reflectron Time-of-Flight Mass Spectrometry. *Int J Mass Spectrom Ion Process* **1994**, *131*, 1–19. https://doi.org/10.1016/0168-1176(93)03891-O.

(49) Weickhardt, C.; Moritz, F.; Grotemeyer, J. Time-of-Flight Mass Spectrometry: State-of the-Art in Chemical Analysis and Molecular Science. *Mass Spectrom Rev* **1996**, *15* (3), 139–162. https://doi.org/10.1002/(SICI)1098-2787(1996)15:3<139::AID-MAS1>3.0.CO;2-J.

(50) Cotter, R. J. *Time-of-Flight Mass Spectrometry*; American Chemical Society: Washington, DC, 1994.

Chapter 2 Quasi-continuous IR-MALDESI source coupled to a Q-TOF mass spectrometer for direct analysis from well plates

Reused with permission from: Arciniega, C.; Garrard, K. P.; Guymon, J. P.; Manni, J. G.; Apffel, A.; Fjeldsted, J. C.; Muddiman, D. C. *Journal of Mass Spectrometry*, **2023**, *58* (1). https://doi.org/10.1002/jms.4902.

2.1 Introduction

High-throughput screening (HTS) is an experimental technique that utilizes automated equipment to process tens of thousands to millions of compounds per day[1]. The analysis time per sample typically is on the sub-second timescale[2]. HTS is commonly used in the pharmaceutical industry for drug discovery due to the need to screen large compound libraries to find hits with a biological or pharmaceutical activity to be used for therapeutic intervention[3,4]. Other applications that require HTS are doping control[5], forensic identification[6], and food safety[7].

Optical methods, such as fluorescence, have been widely used and developed for HTS applications[8]. However, these methods can be inconvenient due to the need of additional chemical derivatization and the common interferences, such as matrix effects, which can result in false positives. Mass spectrometry (MS) has become a popular option due to its high sensitivity, specificity, and no additional labeling preparatory steps[9]. Different methods for sample introduction to the mass spectrometer have been developed which prove the capability of MS for HTS applications[10–16]. Many of these methods are ambient ionization-based techniques, which can be performed in the open air and require minimal sample preparation[17].

Infrared matrix-assisted laser desorption electrospray ionization (IR-MALDESI) is an ambient ionization technique that combines matrix-assisted laser desorption ionization (MALDI) and electrospray ionization (ESI). The sample is placed on a translation stage with a short-wavelength IR laser directed and focused on the meniscus of the sample. The laser ablates the surface of the sample generating a plume of mostly neutrals which interact with the charged droplets from the

orthogonal electrospray resulting in an ESI like ionization mechanism[18]. Therefore, the advantage to produce multiply charged ions allows the analysis of biological samples such as proteins[19]. Different versions of this source have been presented previously using trap-based mass spectrometers[20–22]. This source has been extensively used for mass spectrometry imaging (MSI) applications[23–26].

Previously, the MSI source had been coupled to an Ion Mobility (IM) Quadrupole-Time of Flight (Q-TOF) instrument[27]. This instrument contains an ion trap to accumulate ions before entering the drift tube for gas phase separation. An IM Q-TOF delivers a new dimension which provides structural resolution of ions allowing the identification of isomers. This type of instrument is very useful for the analysis of various biological samples such as plasma, tissue, and biological fluids. However, it is important to consider that the drift tube limits the duty cycle and the dynamic range of the mass spectrometer[28]. An IM scan will have significantly less transients summed per scan which decreases the dynamic range of the instrument[29]. Therefore, turning the ion mobility off and using this instrument in Q-TOF mode increases the duty cycle and dynamic range of the mass spectrometer. Nevertheless, the number of transients summed per scan in Q-TOF mode are less than when using a regular Q-TOF instrument due to the longer path the ions must travel[30]. Consequently, an IM Q-TOF instrument in Q-TOF mode can achieve comparable duty cycles as a regular Q-TOF instrument sacrificing the intensity and the detection of low abundant ions.

IR-MALDESI has also been proven to be a suitable candidate for HTS applications due to its soft ionization characteristics, high salt tolerance, and simple sample preparation using water or ice as a matrix[31]. This source has been previously reported by Radosevich and coworkers[32] to achieve μHTS sampling rates when coupled to an Orbitrap QExactive HF-X mass spectrometer with which they report being able to scan 22.7 samples per second at 7500 Resolving Power (RP)[33]. Orbitrap based instruments need to accumulate ions for a set time before mass analysis. Reducing the time of accumulation increases throughput but sacrifices RP.

Table 2.1. Advantages and disadvantages of Orbitrap and Q-TOF based mass spectrometers [34].

Mass spectrometer	Advantages	Disadvantages
Orbitrap	Significantly higher RP compared to Q-TOF instruments	RP is dependent on *m/z* (bias towards smaller *m/z* ions) and duty cycle
	The dynamic range is not affected by increasing the duty cycle	Lower acquisition rates compared to Q-TOF instruments
	MS^n capabilities[a]	When using a pulsed ionization source, the throughput would be limited by the ion accumulation time and transient time.
Q-TOF	RP is relatively constant across the *m/z* range (larger *m/z* range compared to orbitrap instruments[a])	RP is proportional to the length of the flight tube
	Faster duty cycles that do not depend on RP	RP depends on the instrument optics to deliver a thinner ion packet to the pusher of the TOF
	When using a pulsed ionization source, the throughput would be limited by the ionization event	Increase in acquisition rate results in a loss of sensitivity and dynamic range

[a]Depending on the instrument model

The RP on time of flight (TOF) based instruments, in contrast to Orbitrap mass analyzers, does not depend on *m/z*, therefore it is relatively constant across the entire mass range[34]. Also, the Q-TOF achieves fast duty cycles preserving the dynamic range, high-resolution, and high mass accuracy which is ideal for HTS analyses[35]. **Table 2.1** shows a comparison between Orbitrap and Q-TOF based mass spectrometers, showcasing the advantages and disadvantages of both types of instruments. Given the limitations presented on the Orbitrap mass analyzer, the IR-MALDESI source would benefit from the advantages of the Q-TOF mass spectrometer. In this work, we present in detail the construction of a Quasi-Continuous IR-MALDESI source, its coupling to a commercial Q-TOF mass spectrometer, and its functionality for direct analysis from well plates.

2.2 Experimental

2.2.1 Materials

All aqueous solutions were prepared with deionized water (Millipore Milli-Q; Sigma Aldrich, St. Louis, MO, USA). LC-MS-Grade methanol (MeOH) and acetonitrile (ACN) were purchased from Honeywell (CA, USA). Formic acid (FA) for the electrospray was purchased from Fisher Scientific (Waltham, MA, USA). Caffeine, reserpine, and leucine enkephalin were purchased from Sigma Aldrich (St. Louis, MO, USA). ESI-L Low Concentration Tuning Mix and 0.5 mL 96-well plates were bought from Agilent Technologies (Santa Clara, CA, USA).

2.2.2 Source design

The MALDESI source was developed from previous MALDESI systems[21]. The sample stage consists of a custom-built water-cooled Peltier cold plate bolted onto a 3D translational stage. This source uses a high precision motorized Z stage (GTS30V; Newport Corporation, Irvine, CA, USA) on top of an integrated XY linear motor table (ONE-XY100; Newport Corporation, Irvine, CA, USA). These stages are connected to a motion controller (XPS-RLD4; Newport Corporation, Irvine, CA, USA) which is operated by the in-house developed program RastirZ, which is a modified version of the previously published software RastirX[36]. In contrast to the MSI source, this system does not have an enclosure, since controlling the humidity to form an ice layer is not necessary for direct analysis. The description of the materials used to assemble the source is provided in the **Table A.3**.

2.2.3 Laser and optics

The Quasi-Continuous IR-MALDESI source employs an optical parametric oscillator (OPO) solid-state laser (MSI-0-2970; JGM Associates Inc., MA, USA) that provides nanosecond (7 ns) pulses at a wavelength of 2970 nm. It operates with a laser diode driver (LDD-1) which has on-board circuitry to control the peak current, the current duration, and the number of pulses-per-burst (PPB). This laser has been designed to fire 1 PPB at 100 Hz or less. The parameters used

for the pulse generator are: pulse width = 2.0 msec, 1 PPB, 80% duty cycle, and a burst period of 0.01 s (100 Hz). The measured energy at the sample stage is 0.7 mJ per pulse. The laser is mounted vertically, the beam goes through an anodized aluminum dust tube which contains a CaF_2 concave lens (LC5401; Thorlabs, NJ, USA) to expand the beam. At the end of the path, the beam is focused using a MgF_2 plano-convex lens (LA6002; Thorlabs, NJ, USA). The laser energy was measured with a pyroelectric energy meter (PE25-C; Ophir-Spiricon, UT, USA). It is important to consider that this is a Class IV laser requiring laser safety training and appropriate eye protection while operating the source.

2.2.4 IR-MALDESI-MS analysis

The source was coupled to a Q-TOF mass spectrometer (6545/6546 Q-TOF; Agilent Technologies, Santa Clara, CA, USA). To test the metal capillary the composition of the electrospray was 50% ACN/water, 0.2% FA, and 1uM of the analyte of interest. To test the IR-MALDESI source, the ESI composition was 50% ACN/water, 0.2% FA, and 1uM caffeine. Experiments were carried out with a 3.5 kV spray voltage in positive ion mode. The voltage for the ESI was provided by an external power supply. The Q-TOF capillary voltage (V_{Cap}) and the fragmentor voltage were set to 175 V. The drying gas temperature for the ion transfer capillary was set at 350 ºC. The Q-TOF was set and tuned at “Low Mass Range” (100 *m/z* to 1700 *m/z*). To couple the source to the mass spectrometer we use the remote start connection to trigger the instrument to start and stop a run. The acquisition clock is obtained from the fraction collector port after having a firmware update. Since this is an ambient source located in front of the instrument, the safety interlock of the Q-TOF needs to be bypassed, using a magnet and an iButton, to access the inlet of the mass spectrometer. The iButton is an electronic communication device that tells the software the type of source connected to the front of the instrument. This allows the user to run the instrument without a commercial source enclosure. It must be taken into consideration the potential risk due to the exposure of the high voltage on the outside of the capillary. All the data

was analyzed using MassHunter Qualitative Analysis 10.0 (Agilent Technologies, Santa Clara, CA).

2.3 Results and Discussion

2.3.1 IR-MALDESI source construction

The Quasi-Continuous IR-MALDESI source was constructed and coupled to a commercial Q-TOF mass spectrometer (6545/6546 Q-TOF; Agilent Technologies, Santa Clara CA, USA). **Figure 2.1** shows a schematic representation of the source and its major components.

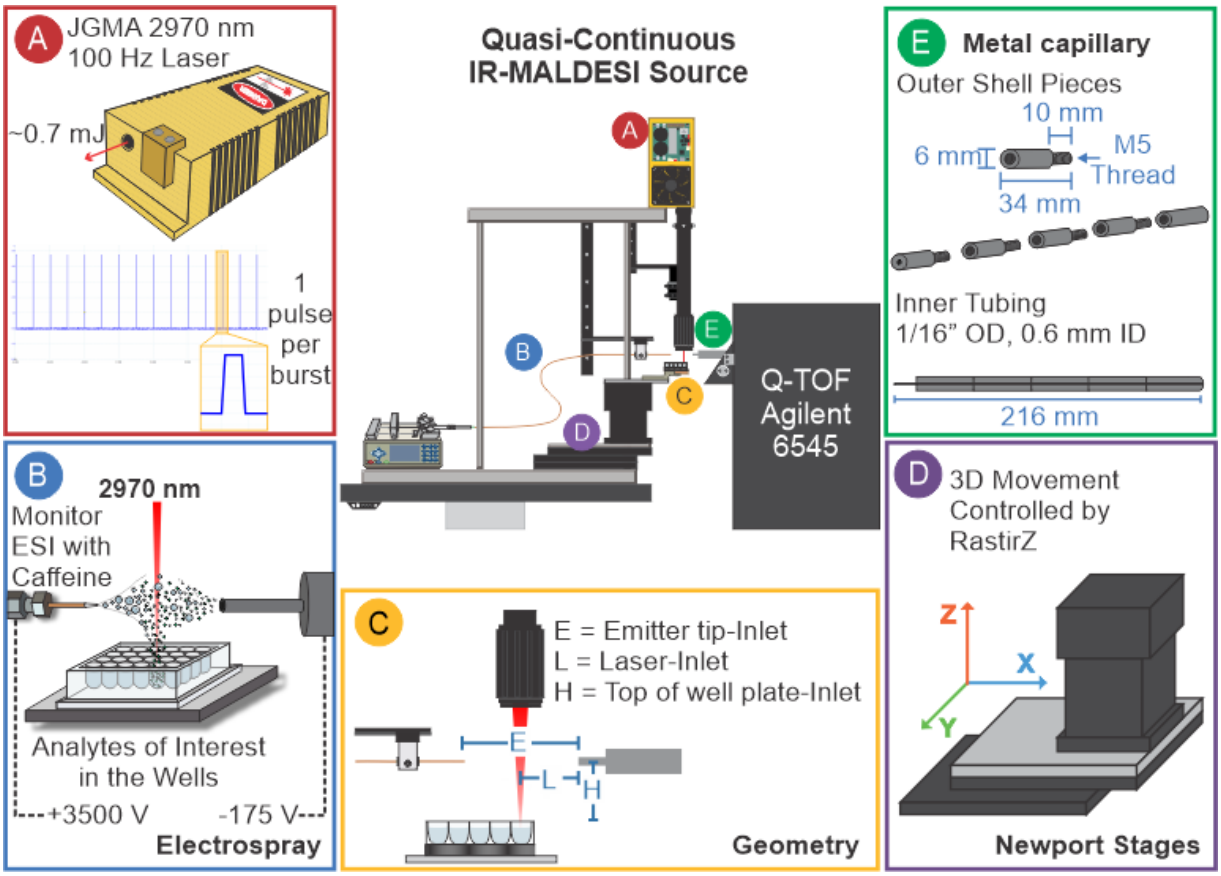

Figure 2.1. Center Top Quasi-continuous IR-MALDESI source. **(A)** 2970 nm laser with a visualization of the burst rate (100 Hz). **(B)** Electrospray orthogonal to the sample and coaxial to the inlet of the mass spectrometer. Caffeine was added to the electrospray to monitor the variability of the signal over time. **(C)** The geometry used to align the emitter tip (E = 15 mm), laser (L = 4 mm), and well plate (H = 14 mm) relative to the inlet of the mass spectrometer. **(D)** Fully automated X, Y, and Z stages controlled by a Newport XPS-RLD controller using the in-house developed program RastirZ. **(E)** A diagram of the metal capillary dimensions used to replace the glass dielectric ion transfer capillary within the Q-TOF.

Considering that a Q-TOF mass spectrometer operates differently than an Orbitrap or FTICR instrument, the components of the IR-MALDESI source have been modified to couple and accommodate to the front end of the instrument. The IR laser used in this source is configured to fire 1 PPB at 100 Hz. This allows for a quasi-continuous ion generation from the sample. For high-throughput screening applications, a faster laser is ideal since the purpose is to analyze as many samples as possible in the shortest amount of time. This laser provides sufficient energy to ablate the sample in 0.02 seconds firing 2 bursts.

To be able to access the entire sample stage in the source the inlet to the instrument was extended. For this purpose, an extended metal capillary was designed and constructed to replace the dielectric capillary inside the desolvation unit of the Q-TOF. This metal capillary was constructed out of a 304/304L stainless steel rod which has a higher thermal conductivity than glass and is able to heat the entire capillary without the need of external heating supplies. Having a uniformly heated capillary increases the desolvation rate of the electrospray charged droplets, therefore increasing ionization efficiency. The capillary consists of two parts: an outer shell and an inner capillary tube. The outer shell is assembled by threaded pieces that connect with each other, with a hollow cavity the diameter of the inner capillary tube. This feature provides the capability to change the length of the capillary by adding or reducing the number of total segments. The inner tube is a stainless-steel tubing with an outer diameter of 1/16” and an inner diameter of 0.6 mm. The inner diameter of the metal capillary is the same as the glass capillary which allows for comparison of the results.

To operate and couple the source to the Q-TOF, the MALDESI source contains an Arduino Nano used to receive and send signals to the different components, a scheme is shown in **Figure 2.2**.

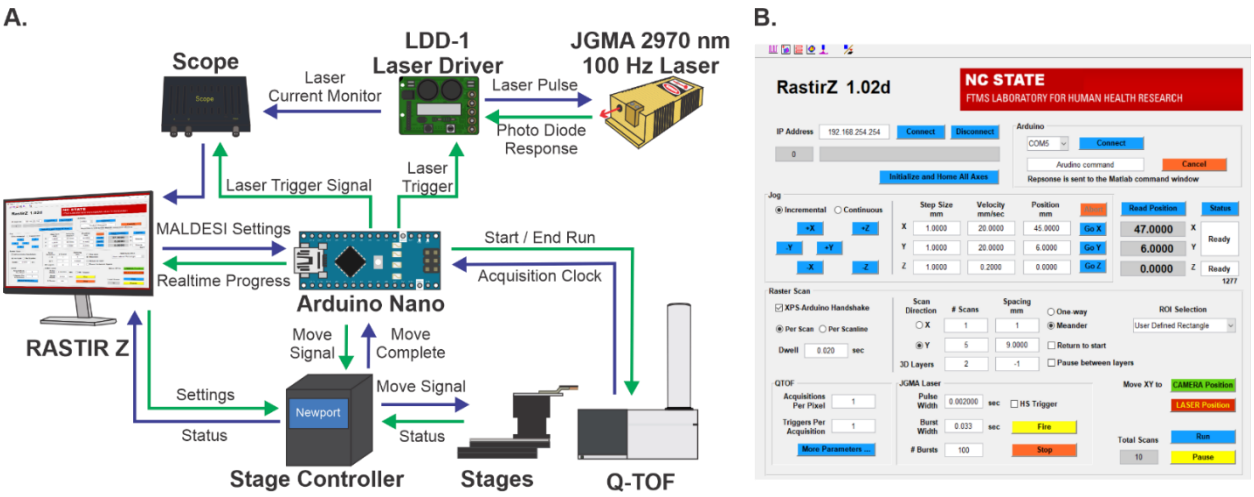

Figure 2.2. (A) Scheme of the communication between the different electronic components of the Quasi-Continuous IR-MALDESI source. An Arduino Nano is used to synchronize axes motion with triggering the laser using the in-house developed program RastirZ. **(B)** Screenshot of the RastirZ Graphical User Interface (GUI). This GUI easily enables the user to fire the laser and jog the axis, move to a desired position, or setup a Raster Scan pattern.

The user programs the MALDESI settings using the RastirZ software, where they can choose how to move the stages and fire the laser. The Arduino Nano also communicates with the Q-TOF to send an external trigger to start recording data. **Figure 2.3** indicates the timing of the signals to and from each IR-MALDESI-MS component. The signals illustrate acquiring data from two adjacent wells (samples) in an experiment. To increase throughput, the Arduino sends one Start signal to the instrument before the first well, and the system keeps recording until the last well has been analyzed.

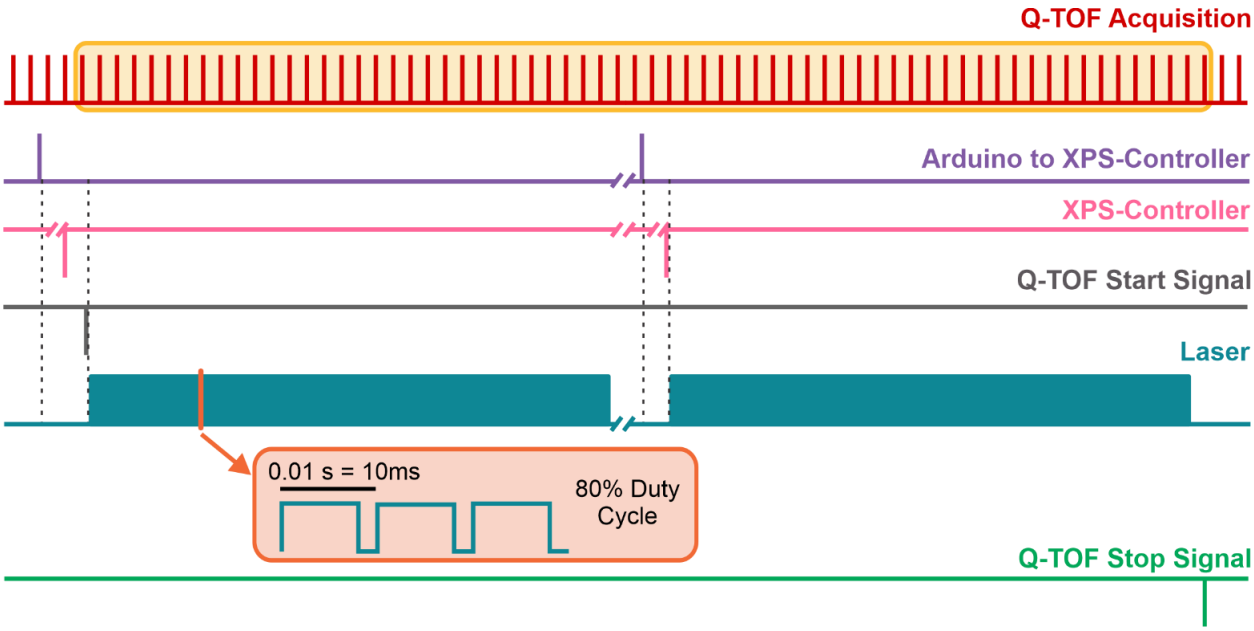

Figure 2.3. Synchronization timing for collecting IR-MALDESI data with the Agilent Q-TOF. The Q-TOF acquisition signal is set to 3 scans/sec and the width of each pulse is 100 µsec. The Arduino to XPS-Controller signal has a pulse width of 30 msec. The XPS-Controller signal has a pulse width is 20 msec. The Q-TOF start and stop signals each have a pulse width of 500 msec. The laser pulses have a burst width of 10 msec firing 1 PPB at 100 Hz with 80% duty cycle. The yellow section shows the acquisition clock while the Q-TOF is recording data.

The broken axis in the middle shows a variable delay between the scans of the first well and the scans of the second well. The delay depends on the sampling rate of the mass spectrometer. The acquisition rate of the Q-TOF is variable and can be set in the “Method Editor” section of the instrument software. For the experiments shown in this work, the acquisition rate was set to 3 scans/sec. The Q-TOF constantly acquires data and resets the scan clock to 0 when it receives a start signal to record data. The trigger signal from the Arduino Nano to the XPS-Controller initiates stage movement. Afterwards, the XPS-controller sends a signal to the Arduino indicating that stage motion is complete. The delay shown in this signal as a broken axis depends on the velocity and distance the stages travel. The Newport ONE-XY linear motor axes are capable of 400 mm/sec velocity and 2.94 m/sec^2 acceleration. After the XPS-Controller confirms position, the Arduino sends the start signal to the Q-TOF to begin recording data. The Arduino then triggers the laser, and it starts firing 1 pulse-per-burst (ppb) at 100 Hz. The number of pulses

per burst, pulse width, duty cycle, burst width and number of bursts can be specified up to a maximum pulse rate of 10 kHz and a maximum burst rate of 100 Hz.

We can find the timing difference between the signal of the Arduino to the XPS-Controller (purple) and the laser trigger (teal) are different for the first and second well. The order of events after the analysis of the first well follows below: 1) Arduino sends a signal to the XPS controller to move the stage to the next well, shown in purple line. 2) After the stage moves to the position, the XPS controller returns a signal to confirm the position, shown in pink line. 3) The laser is triggered to fire the desired number of pulses, shown in teal rectangle. During this process, the Q-TOF is continuously operating, which largely reduces the timing between wells. Another start signal sent to Q-TOF to begin recording data of the second well would cause a delay between analysis of the first and second well. The Stop signal is sent to the instrument after all the desired wells have been analyzed.

2.3.2 Comparing the heated metal capillary and glass dielectric capillary

Using the IR-MALDESI electrospray, reserpine, leucine enkephalin, and tune mix were analyzed to compare the glass dielectric and metal capillaries. For both experiments, an external power supply was used to set the high voltage on the emitter tip. The voltage on the capillary and fragmentor were set to 175V because the metal capillary will conduct the voltage from one end to the other. **Figure 2.4** shows the extracted ion chromatogram (EIC) and the mass spectrum of reserpine, leucine enkephalin, and each compound in the tune mix. As predicted, the metal capillary resulted in higher measured signal for each analyte tested, relative to the glass dielectric capillary. This is likely due to a more uniform heat distribution across the metal capillary resulting in a higher desolvation rate. In the case of **Figure 2.4A**, the electrospray was less stable with the metal capillary than the glass capillary. However, it is also worth considering that the stability of the electrospray varies as ambient conditions such as humidity changes. Therefore, we cannot conclude that the variability of the signal in this experiment is solely due to the metal capillary or

ambient reasons. Moreover, in **Figure 2.4B** we can see that the stability of the signal using the metal capillary is comparable to the glass capillary.

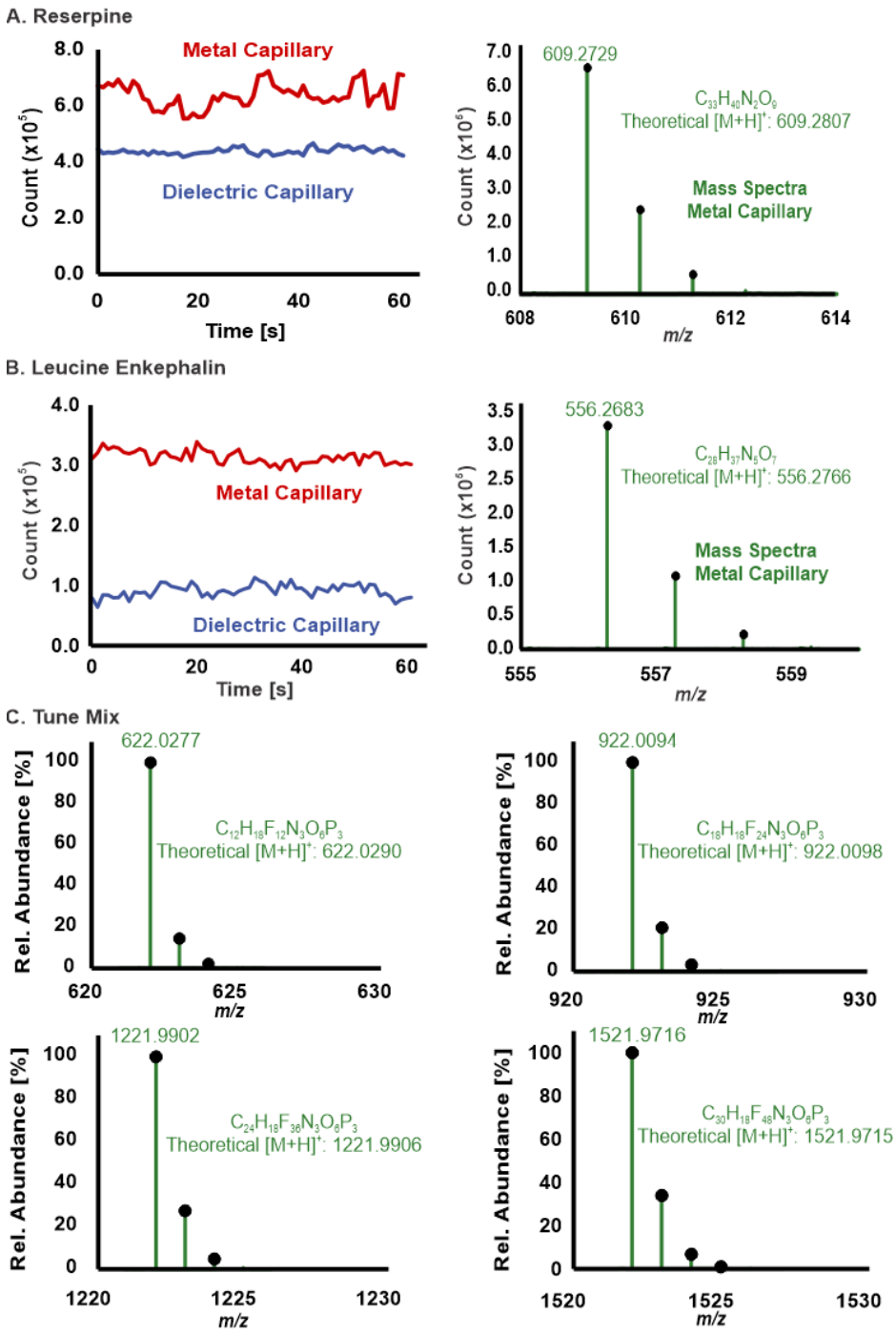

Figure 2.4. (A) EIC and Spectrum of Reserpine acquired with the metal and glass capillaries by ESI. **(B)** EIC and Spectrum of Leucine enkephalin acquired with the metal and glass capillaries

by ESI. **(C)** Spectra of the main ions in the Tune Mix showing mass accuracy acquired with the metal capillary by ESI

We can see that for reserpine we have a 1.5x increase in signal while for leucine enkephalin we have 3 times more signal abundance using the metal capillary. The difference in increase between these two molecules could be due to their ionization efficiencies, but we have insufficient information to be confident of that conclusion. Regarding mass accuracy, we can see that the main ions of the tune mix have ± 2ppm, considering we are not using an internal reference. Overall, we can say that the metal capillary works as well or better than the dielectric glass capillary at introducing ions into the mass spectrometer. Additionally, the metal capillary provides the extension needed to run IR-MALDESI with the Q-TOF.

To prove the functionality and capabilities of the IR-MALDESI source, tune mix diluted to 50% with water was added to a 0.5mL 96-well plate. A 1 μM caffeine solution diluted in ESI solvent was added to the electrospray to monitor its stability and variability in time. Two experiments were performed, one firing bursts for 10 s (**Figure 2.5A**), and the second one firing bursts continuously for 60 s (**Figure 2.5B**). For **Figure 2.5A**, the laser was fired twice over 120 s. In green we can see the IR-MALDESI mass spectra for both replicates. For **Figure 2.5B**, the laser was fired once for a longer period of time. The two mass spectra shown are representations of the IR-MALDESI signal at 2 different times showing the highest abundance and the lowest abundance sections of the EIC. The EIC shows spikes due to the acquisition time of the instrument and the quasi-continuous ion generation from the source. However, we can see that even when the abundances are lower, we obtain good mass spectra with high mass accuracy.

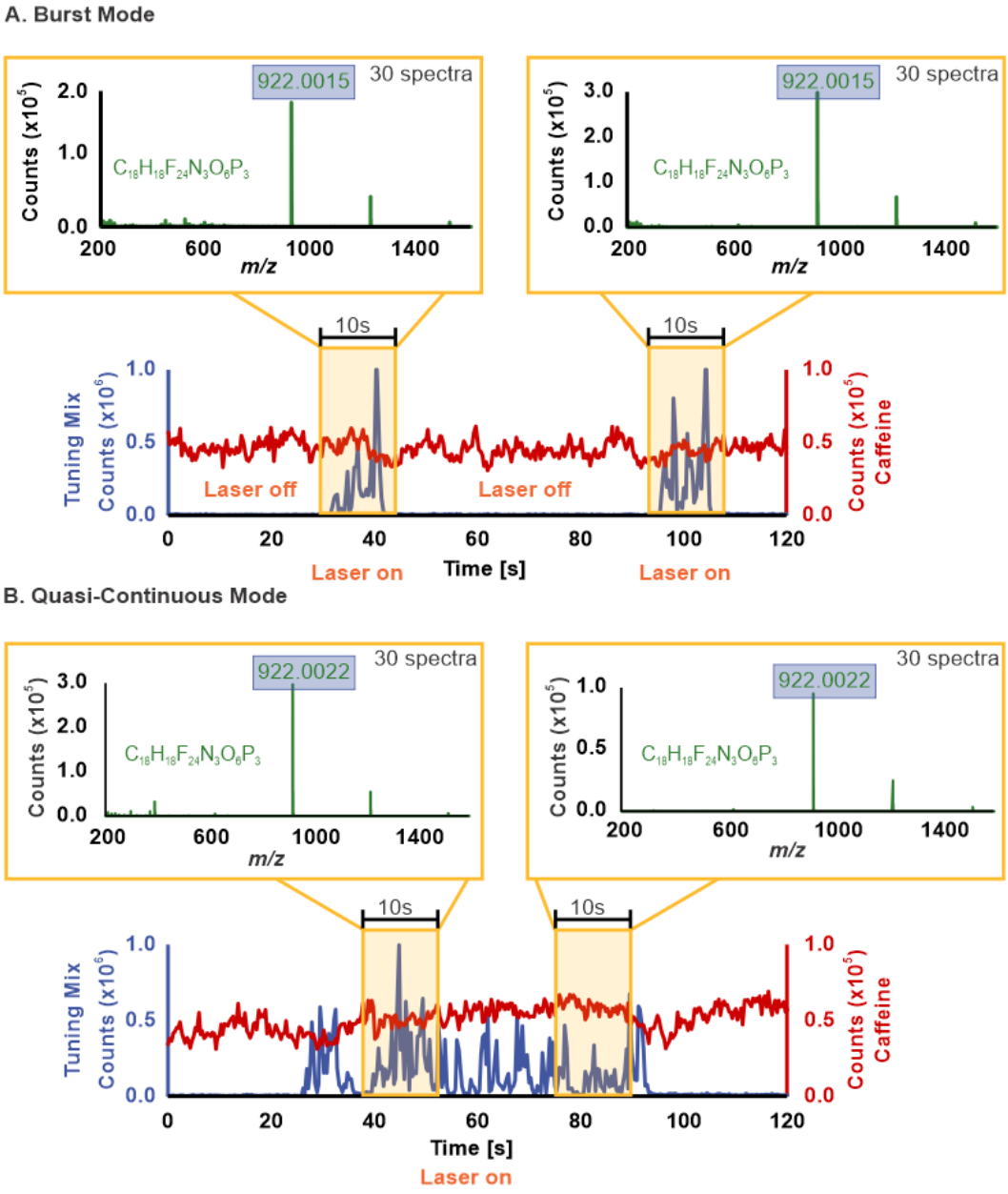

Figure 2.5. (A) The burst mode consists of firing the laser for a short period of time intermittently. **(B)** The Quasi-Continuous mode consists of firing the laser for a long period of time. This mode demonstrates the capability of the source to ionize an analyte quasi-continuously.

We can say that this ionization source has two modes of operation given by the laser: burst and quasi-continuous. Each mode could be used for different applications. The burst mode is useful for imaging purposes whilst the quasi-continuous mode for HTS analyses. Laser based sources operate as pulsed ionization sources. However, this MALDESI source presents a new capability to operate as a quasi-continuous ionization source given by the speed of the laser

bursts. This MS platform could lead to an increase in the throughput analysis by IR-MALDESI MS.

2.4 Conclusions

A novel quasi-continuous IR-MALDESI source was developed and coupled to a Q-TOF mass spectrometer to overcome limitations of IR-MALDESI coupled to Orbitrap mass spectrometers. This instrument provides the advantage of having high acquisition rates maintaining the resolving power constant over the entire *m/z* range, which is especially beneficial to analysis of macromolecules (*e.g.*, proteins). The laser mounted in this source fires 1 PPB at 100 Hz and provides sufficient energy to ablate the sample with a single pulse. Firing this laser for a long period of time allows this source to generate a quasi-continuous ion beam, ideal for coupling to a continuous mass analyzer. Additionally, an extended metal capillary was built to extend the inlet of the Q-TOF which increased measured signal compared to the conventionally used glass dielectric capillary by Agilent. The functionality and capabilities of this source were proven in this work demonstrating a new system for direct analysis from well plates. The capabilities of this source show the potential it has for high-throughput screening and other applications. In future work, the source will be further characterized with this mass spectrometer using a broad range of molecules and biological samples.

2.5 References

(1) Attene-Ramos, M. S.; Austin, C. P.; Xia, M. High Throughput Screening. In *Encyclopedia of Toxicology: Third Edition*; Elsevier, 2014; pp 916–917. https://doi.org/10.1016/B978-0-12-386454-3.00209-8.

(2) Haslam, C.; Hellicar, J.; Dunn, A.; Fuetterer, A.; Hardy, N.; Marshall, P.; Paape, R.; Pemberton, M.; Resemannand, A.; Leveridge, M. The Evolution of MALDI-TOF Mass Spectrometry toward Ultra-High-Throughput Screening: 1536-Well Format and Beyond. *J Biomol Screen* **2016**, *21* (2), 176–186. https://doi.org/10.1177/1087057115608605.

(3) Sundberg, S. High-Throughput and Ultra-High-Throughput Screening: Solution- and Cell-Based Approaches. *Curr Opin Biotechnol* **2000**, *11* (1), 47–53. https://doi.org/10.1016/S0958-1669(99)00051-8.

(4) Hertzberg, R. P.; Pope, A. J. High-Throughput Screening: New Technology for the 21st Century. *Curr Opin Chem Biol* **2000**, *4* (4), 445–451. https://doi.org/10.1016/S1367-5931(00)00110-1.

(5) Musenga, A.; Cowan, D. A. Use of Ultra-High Pressure Liquid Chromatography Coupled to High Resolution Mass Spectrometry for Fast Screening in High Throughput Doping Control. *J Chromatogr A* **2013**, *1288*, 82–95. https://doi.org/10.1016/j.chroma.2013.03.006.

(6) Pan, M.; Xiang, P.; Yu, Z.; Zhao, Y.; Yan, H. Development of a High-Throughput Screening Analysis for 288 Drugs and Poisons in Human Blood Using Orbitrap Technology with Gas Chromatography-High Resolution Accurate Mass Spectrometry. *J Chromatogr A* **2019**, *1587*, 209–226. https://doi.org/10.1016/j.chroma.2018.12.022.

(7) Yan, Y.; Ai, L.; Zhang, H.; Kang, W.; Zhang, Y.; Lian, K. Development an Automated and High-Throughput Analytical Platform for Screening 39 Glucocorticoids in Animal-Derived Food for Doping Control. *Microchemical Journal* **2021**, *165*. https://doi.org/10.1016/j.microc.2021.106142.

(8) Eggeling, C.; Brand, L.; Ullmann, D.; Jäger, S. Highly Sensitive Fluorescence Detection Technology Currently Available for HTS. *Drug Discov Today* **2003**, *8* (14), 632–641. https://doi.org/10.1016/S1359-6446(03)02752-1.

(9) McLaren, D. G.; Shah, V.; Wisniewski, T.; Ghislain, L.; Liu, C.; Zhang, H.; Saldanha, S. A. High-Throughput Mass Spectrometry for Hit Identification: Current Landscape and Future Perspectives. *SLAS Discovery*. SAGE Publications Inc. February 1, 2021, pp 168–191. https://doi.org/10.1177/2472555220980696.

(10) Häbe, T. T.; Liu, C.; Covey, T. R.; Simon, R. P.; Reindl, W.; Büttner, F. H.; Winter, M.; Bischoff, D.; Luippold, A. H.; Runge, F. Ultrahigh-Throughput ESI-MS: Sampling Pushed to Six Samples per Second by Acoustic Ejection Mass Spectrometry. *Anal Chem* **2020**, *92* (18), 12242–12249. https://doi.org/10.1021/acs.analchem.0c01632.

(11) Simon, R. P.; Häbe, T. T.; Ries, R.; Winter, M.; Wang, Y.; Fernández-Montalván, A.; Bischoff, D.; Runge, F.; Reindl, W.; Luippold, A. H.; Büttner, F. H. Acoustic Ejection Mass Spectrometry: A Fully Automatable Technology for High-Throughput Screening in Drug Discovery. *SLAS Discovery* **2021**, *26* (8), 961–973. https://doi.org/10.1177/24725552211028135.

(12) Pearson, L. A.; Green, C. J.; Lin, D.; Petit, A. P.; Gray, D. W.; Cowling, V. H.; Fordyce, E. A. F. Development of a High-Throughput Screening Assay to Identify Inhibitors of the SARS-CoV-2 Guanine-N7-Methyltransferase Using RapidFire Mass Spectrometry. *SLAS Discovery* **2021**, *26* (6), 749–756. https://doi.org/10.1177/24725552211000652.

(13) Simon, R. P.; Winter, M.; Kleiner, C.; Wehrle, L.; Karnath, M.; Ries, R.; Zeeb, M.; Schnapp, G.; Fiegen, D.; Häbe, T. T.; Runge, F.; Bretschneider, T.; Luippold, A. H.; Bischoff, D.; Reindl, W.; Büttner, F. H. MALDI-TOF-Based Affinity Selection Mass Spectrometry for Automated Screening of Protein–Ligand Interactions at High Throughput. *SLAS Discovery* **2021**, *26* (1), 44–57. https://doi.org/10.1177/2472555220959266.

(14) Wei, Z.; Xie, Z.; Kuvelkar, R.; Shah, V.; Bateman, K.; McLaren, D. G.; Cooks, R. G. High-Throughput Bioassays Using “Dip-and-Go” Multiplexed Electrospray Mass Spectrometry. *Angewandte Chemie* **2019**, *131* (49), 17758–17762. https://doi.org/10.1002/ange.201909047.

(15) Logsdon, D. L.; Li, Y.; Paschoal Sobreira, T. J.; Ferreira, C. R.; Thompson, D. H.; Cooks, R. G. High-Throughput Screening of Reductive Amination Reactions Using Desorption Electrospray Ionization Mass Spectrometry. *Org Process Res Dev* **2020**, *24* (9), 1647–1657. https://doi.org/10.1021/acs.oprd.0c00230.

(16) Khaled, A.; Belinato, J. R.; Pawliszyn, J. Rapid and High-Throughput Screening of Multi-Residue Pharmaceutical Drugs in Bovine Tissue Using Solid Phase Microextraction and Direct Analysis in Real Time-Tandem Mass Spectrometry (SPME-DART-MS/MS). *Talanta* **2020**, *217*. https://doi.org/10.1016/j.talanta.2020.121095.

(17) Li, L. P.; Feng, B. S.; Yang, J. W.; Chang, C. L.; Bai, Y.; Liu, H. W. Applications of Ambient Mass Spectrometry in High-Throughput Screening. *Analyst*. Royal Society of Chemistry June 7, 2013, pp 3097–3103. https://doi.org/10.1039/c3an00119a.

(18) Dixon, R. B.; Muddiman, D. C. Study of the Ionization Mechanism in Hybrid Laser Based Desorption Techniques. *Analyst* **2010**, *135* (5), 880–882. https://doi.org/10.1039/b926422a.

(19) Ho, C. S.; Lam, C. W. K.; Chan, M. H. M.; Cheung, R. C. K.; Law, L. K.; Lit, L. C. W.; Ng, K. F.; Suen, M. W. M.; Tai, H. L. Electrospray Ionisation Mass Spectrometry: Principles and Clinical Applications. *Clin Biochem Rev* **2003**, *24* (1), 3–12.

(20) Knizner, K. T.; Guymon, J. P.; Garrard, K. P.; Bouvrée, G.; Manni, J.; Hauschild, J.-P.; Strupat, K.; Fort, K. L.; Earley, L.; Wouters, E. R.; Pu, F.; Radosevich, A. J.; Elsen, N. L.; Williams, J. D.; Pankow, M. R.; Muddiman, D. C. Next-Generation Infrared Matrix-Assisted Laser Desorption Electrospray Ionization Source for Mass Spectrometry Imaging and High-Throughput Screening. *J Am Soc Mass Spectrom* **2022**, *33* (11), 2070–2077. https://doi.org/10.1021/jasms.2c00178.

(21) Robichaud, G.; Barry, J. A.; Garrard, K. P.; Muddiman, D. C. Infrared Matrix-Assisted Laser Desorption Electrospray Ionization (IR-MALDESI) Imaging Source Coupled to a FT-ICR Mass Spectrometer. *J Am Soc Mass Spectrom* **2013**, *24* (1), 92–100. https://doi.org/10.1007/s13361-012-0505-9.

(22) Sampson, J. S.; Murray, K. K.; Muddiman, D. C. Intact and Top-down Characterization of Biomolecules and Direct Analysis Using Infrared Matrix-Assisted Laser Desorption Electrospray Ionization Coupled to FT-ICR Mass Spectrometry. *J Am Soc Mass Spectrom* **2009**, *20* (4), 667–673. https://doi.org/10.1016/j.jasms.2008.12.003.

(23) Bai, H.; Linder, K. E.; Muddiman, D. C. Three-Dimensional (3D) Imaging of Lipids in Skin Tissues with Infrared Matrix-Assisted Laser Desorption Electrospray Ionization (MALDESI) Mass Spectrometry. *Anal Bioanal Chem* **2021**, *413* (10), 2793–2801. https://doi.org/10.1007/S00216-020-03105-6/FIGURES/6.

(24) Mwangi, J. N.; William M. Gilliland, J.; White, N.; Sykes, C.; Poliseno, A.; Knudtson, K. A.; Hightow-Weidman, L.; Kashuba, A. D. M.; Rosen, E. P. Mass Spectroscopy Imaging of Hair Strands Captures Short-Term and Long-Term Changes in Emtricitabine Adherence. *Antimicrob Agents Chemother* **2022**. https://doi.org/10.1128/AAC.02176-21.

(25) Pace, C. L.; Simmons, J.; Kelly, R. T.; Muddiman, D. C. Multimodal Mass Spectrometry Imaging of Rat Brain Using IR-MALDESI and NanoPOTS-LC-MS/MS. *J Proteome Res* **2022**, *21* (3), 713–720. https://doi.org/10.1021/ACS.JPROTEOME.1C00641/SUPPL_FILE/PR1C00641_SI_003.XLSX.

(26) Mellinger, A. L.; Muddiman, D. C.; Gamcsik, M. P. Highlighting Functional Mass Spectrometry Imaging Methods in Bioanalysis. *J Proteome Res* **2022**, *21* (8), 1800–1807. https://doi.org/10.1021/acs.jproteome.2c00220.

(27) Ekelöf, M.; Dodds, J.; Khodjaniyazova, S.; Garrard, K. P.; Baker, E. S.; Muddiman, D. C. Coupling IR-MALDESI with Drift Tube Ion Mobility-Mass Spectrometry for High-Throughput Screening and Imaging Applications. *J Am Soc Mass Spectrom* **2020**, *31* (3), 642–650. https://doi.org/10.1021/JASMS.9B00081/SUPPL_FILE/JS9B00081_SI_001.PDF.

(28) Delafield, D. G.; Lu, G.; Kaminsky, C. J.; Li, L. High-End Ion Mobility Mass Spectrometry: A Current Review of Analytical Capacity in Omics Applications and Structural Investigations. *TrAC - Trends in Analytical Chemistry* **2022**, *157*. https://doi.org/10.1016/j.trac.2022.116761.

(29) Stow, S. M.; Fjeldsted, J. C. Fundamentals of Uniform-Field Drift Tube Ion Mobility and Collision Cross Section. In *Ion Mobility-Mass Spectrometry. Fundamentals and Applications*; Royal Society of Chemistry, 2021; Vol. 11.

(30) Causon, T. J.; Kurulugama, R. T.; Hann, S. Drift-Tube Ion Mobility-Mass Spectrometry for Nontargeted 'Omics. In *Ion Mobility-Mass Spectrometry. Methods in Molecular Biology*; Humana: New York, 2020; Vol. 2084, pp 79–94. https://doi.org/10.1007/978-1-0716-0030-6_4.

(31) Caleb Bagley, M.; Garrard, K. P.; Muddiman, D. C. The Development and Application of Matrix Assisted Laser Desorption Electrospray Ionization: The Teenage Years. *Mass Spectrom Rev* **2021**, mas.21696. https://doi.org/10.1002/mas.21696.

(32) Pu, F.; Radosevich, A. J.; Sawicki, J. W.; Chang-Yen, D.; Talaty, N. N.; Gopalakrishnan, S. M.; Williams, J. D.; Elsen, N. L. High-Throughput Label-Free Biochemical Assays Using Infrared Matrix-Assisted Desorption Electrospray Ionization Mass Spectrometry. *Anal Chem* **2021**, *93* (17), 6792–6800. https://doi.org/10.1021/ACS.ANALCHEM.1C00737.

(33) Radosevich, A. J.; Pu, F.; Chang-Yen, D.; Sawicki, J. W.; Talaty, N. N.; Elsen, N. L.; Williams, J. D.; Pan, J. Y. Ultra-High-Throughput Ambient MS: Direct Analysis at 22 Samples per Second by Infrared Matrix-Assisted Laser Desorption Electrospray Ionization Mass Spectrometry. *Anal Chem* **2022**, *94* (12), 4913–4918. https://doi.org/10.1021/ACS.ANALCHEM.1C04605.

(34) Eichhorn, P.; Pérez, S.; Barceló, D. Time-of-Flight Mass Spectrometry Versus Orbitrap-Based Mass Spectrometry for the Screening and Identification of Drugs and Metabolites: Is There a Winner? In *Comprehensive Analytical Chemistry*; Elsevier B.V., 2012; Vol. 58, pp 217–272. https://doi.org/10.1016/B978-0-444-53810-9.00009-2.

(35) Han, J.; Datla, R.; Chan, S.; Borchers, C. H. Mass Spectrometry-Based Technologies for High-Throughput Metabolomics. *Bioanalysis*. Future Science Ltd 2009, pp 1665–1684. https://doi.org/10.4155/bio.09.158.

(36) Garrard, K. P.; Ekelöf, M.; Khodjaniyazova, S.; Bagley, M. C.; Muddiman, D. C. A Versatile Platform for Mass Spectrometry Imaging of Arbitrary Spatial Patterns. *J Am Soc Mass Spectrom* **2020**, *31* (12), 2547–2552. https://doi.org/10.1021/JASMS.0C00128.

Chapter 3 A Mass Spectrometry Imaging Centric Database for High-Resolution Accurate Mass Identifications in Biological Applications

3.1 Introduction

Mass spectrometry imaging (MSI) is a powerful analytical technique that enables the identification of spatially resolved compounds in a sample[1]. As a result, we obtain molecular images by combining the *x*, *y* and *z* locations of a sample with their corresponding mass spectra. MSI is a direct analysis technique which requires minimal to no sample preparation and can be performed under vacuum or at atmospheric pressure. Given that MSI doesn't use a previous separation technique, the data can be very complex and difficult to analyze. Furthermore, this technique requires a high-resolution accurate mass (HRAM) mass spectrometer to be separate multiple molecules in the same *m/z* range[2]. It is widely used in the study of diseases by sampling tissue sections to analyze biological molecules such as peptides[3,4], lipids[5,6], metabolites[7,8], and *N*-linked glycans[9].

Several types of ionization sources have been utilized for this purpose[10,11]. Laser based ionization techniques, such as MALDI[12] and IR-MALDESI[13], have become popular for this application. MALDI requires the application of an organic matrix on top of the tissue. The desorption event happens on the surface of the tissue, generating pixels that form an image. With this ionization technique mostly singly-charged ions are observed, limiting the types of adducts that can be formed. On the other hand, IR-MALDESI uses an ice matrix on top of the tissue to enhance the sample ablation process. The laser completely ablates the sample, removing a consistent volume of tissue and generating voxels that form an image. Given the nature of IR-MALDESI, multiply-charged species are easily detected. This enables detection of multiple adducts of the same molecule in a single mass spectrum.

A variety of software platforms exist to visualize MSI data and create ion images in the form of heatmaps. Additionally, some of these platforms perform automated annotations by

searching databases[14]. MSiReader was introduced in 2013 as an open source developed to process HRAM MSI data[13,15,16]. During the last decade, it has become popular in the MSI community for its visualization and analytics. It contains tools to pre-process and visualize data, plus perform QA/QC, annotations, quantification, and statistical analysis. However, the database (DB) for annotations contains a small number of lipid ions identified in a healthy hen ovarian tissue by shotgun lipidomics. Although, the DB is user expandable, it has been designed for lipids. Given the diversity of samples and molecules analyzed by MSI, there is a need for a new DB.

Moreover, the most popular platform for annotations is METASPACE. This software, introduced by Aleksadrov[17], uses a wide variety of databases (DBs) allowing the annotations of biological molecules (*i.e.,* metabolites, lipids, *N*-glycans). Additionally, datasets are public after publication and users benefit from the annotations submitted by others. These DBs have been constructed with liquid chromatography tandem mass spectrometry (LC-MS/MS) data and contain the neutral species of each molecule. The user selects the ionization mode and the desired adducts to search the database and annotate the data, with additional sample analysis information. Provided that MALDI is a commercial source, and it's the most popular source used for MSI, this software has been developed around it. Therefore, the presented adducts are limited to singly-charged species.

Moreover, the software uses two types of scoring algorithms to determine whether an annotation is correct or incorrect. The first is the MSM score, which is a combination of three scores, spatial chaos (ρ_{chaos}), spatial isotope ($\rho_{spatial}$), and spectral isotope ($\rho_{spectral}$)[17]. Spatial chaos quantifies the structure of an ion image, spatial isotope measures the spatial similarity between isotopes of the same ion, and the spectral isotope quantifies the similarity between the predicted isotopic distribution and the measured spatial intensities. The second type of scoring is a False Discovery Rate (FDR), which uses a target-decoy approach to discard false annotations that have passed the MSM score[17]. The decoy set is generated by creating implausible adducts of the same

molecular formulas (one adduct per formula), calculating the MSM score, and removing the adducts below the MSM cutoff. The user selects a desired FDR value which removes the annotations above that threshold. Unfortunately, this filtering system may eliminate true annotations with low scores.

Over the years it has been shown that the use of LC-MS/MS DBs does not accurately represent the molecules observed in MSI experiments due to their complexity (*e.g.,* LipidMaps contains over 25000 entries from which *ca.,* 1000 are observed by MSI). Therefore, the need for an MSI centric DB is of great importance in the field. In addition, the use of ESI hybrid ionization techniques, such as IR-MALDESI, has shown the need for a DB searching algorithm that supports multiply-charged adducts. Herein, we present a customizable MSI centric neutral DB agnostic of the molecule type and ionization technique. It is coupled to a searching tool for annotations which supports multiply-charged species by allowing the user to customize the desired adducts.

3.2 Customizable DB and searching algorithm

The DB entries have been added using MSI data by IR-MALDESI coupled to an Orbitrap Exploris 240 mass spectrometer. **Table 3.1** shows an example of the DB, with the required information to add new molecules. This is a neutral DB that works with the monoisotopic mass of each molecule. Additionally, a tool will allow customization by users to add new observed molecules for future annotations. The sample type can be tissue or direct analysis. This category has been specially added for *N*-linked glycans, where the reducing end of the molecule changes due to the cleaving of the glycan in solution vs tissue.

Table 3.1. Example of database entries

Molecule Name(s)	Formula	Monoisotopic Mass	Molecular class	Sample type	Lipid category	Lipid Class	Fatty Acid(s)
Lactaldehyde	C3H6O2	74.0368	Metabolites	Tissue			
Imidazole-4-acetaldehyde	C5H6N2O	110.0480	Neurotransmitters	Tissue			
PC(2:0)	C12H24NO8P	341.1240	Lipids	Tissue	GP	PC	(2:0)
Cholesterol	C27H46O	386.3549	Lipids	Tissue	ST		
H3N5S1	C69H114O49N6	1810.6613	N-Linked Glycans	Tissue			
H6N5S3	C109H178O79N8	2863.0157	N-Linked Glycans	Direct analysis			

The graphical user interface (GUI) for the searching tool is presented in **Figure 3.1**. This interface allows the user to input a list of *m/z* values to compare with the DB find matches. It also contains a section to specify sample information such as experiment conditions, replicate number, and so on. The MS Analysis section contains dropdown lists that allow the user to select the options. The adduct(s) list changes with the ionization mode and allows multiple selections. Thus, the user can select as many adducts as desired. The list of adducts can be customized to allow for new ions that have not been considered. This capability makes this searching tool agnostic of the ionization technique, enabling the use of multiply-charged species.

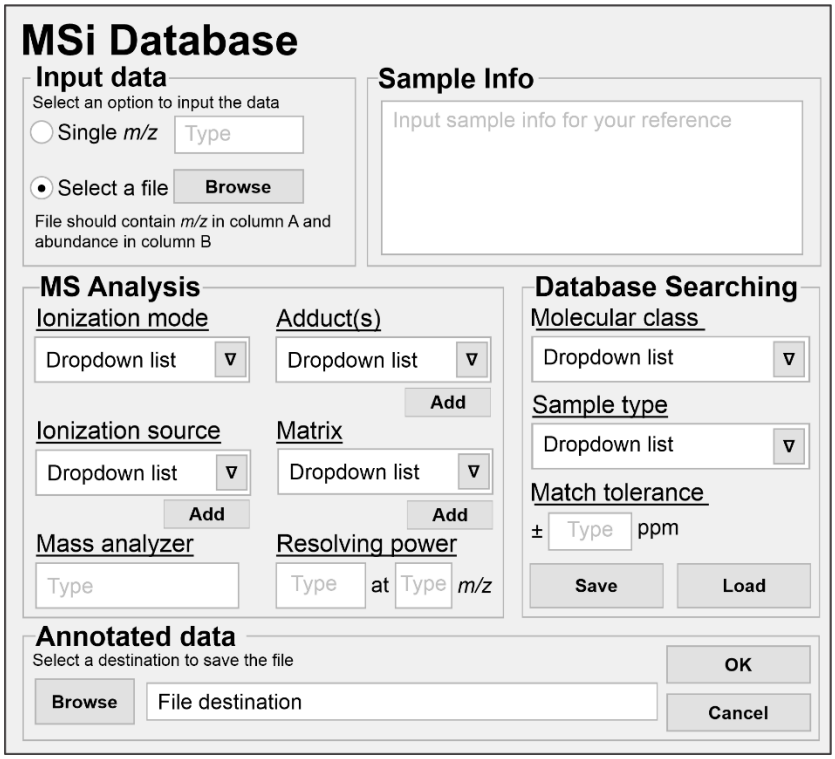

Figure 3.1. Graphical User Interface MSi Database.

Moreover, the Database Searching section contains the three main filters to search the database. The match tolerance limits the annotations within this interval. For HRAM data, it is recommended to use the mass accuracy provided by the instrument (*e.g.,* 1 ppm). Increasing the match tolerance will provide more annotations. However, the confidence of those annotations is

likely to be lower. The output file contains three sheets: info, annotations, and unmatched queries. The annotations table will have the list of query *m/z*, abundance, theoretical *m/z*, mass measurement accuracy (MMA) in ppm, adduct, charge state(s), and the DB information. **Figure 3.2** shows the steps followed by the algorithm to create annotations from the generated adducts.

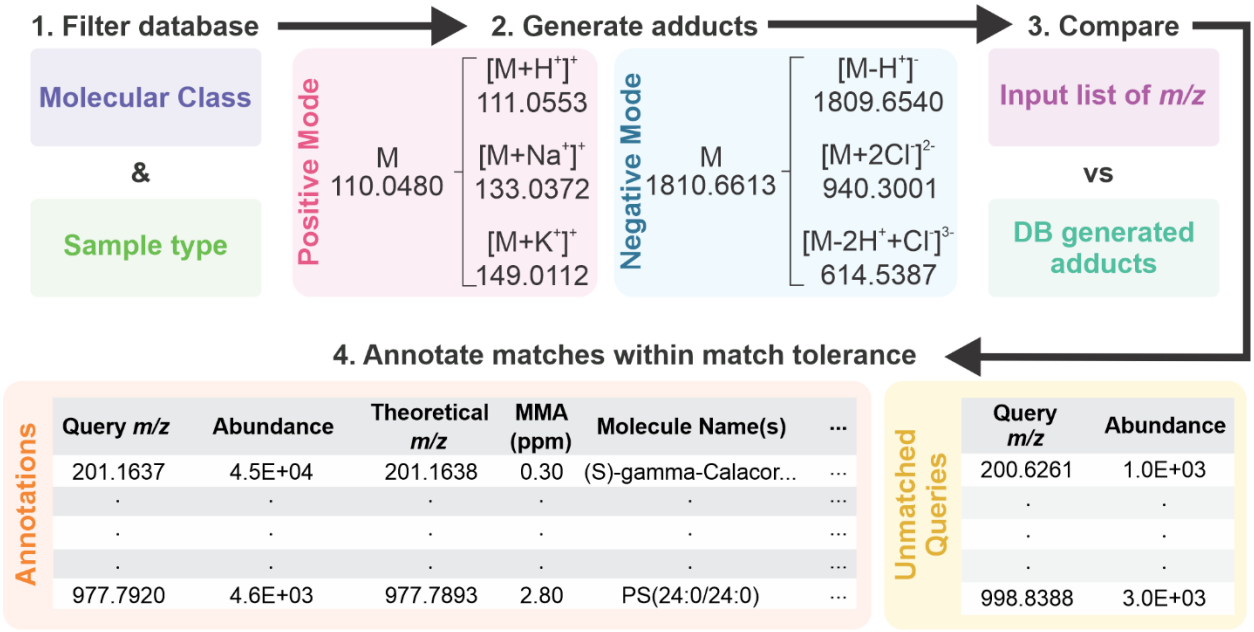

Figure 3.2. Search algorithm workflow.

3.3 Practical example: annotating *N*-linked glycans

MSI experiments can be performed to study a single region of interest (ROI) or compare multiple ROIs to find the molecular differences. Hence, an MSI data analysis workflow is shown in **Figure 3.3**. This workflow includes the process for both types of experiments. It uses MSiReader's tools to process and analyze the data.

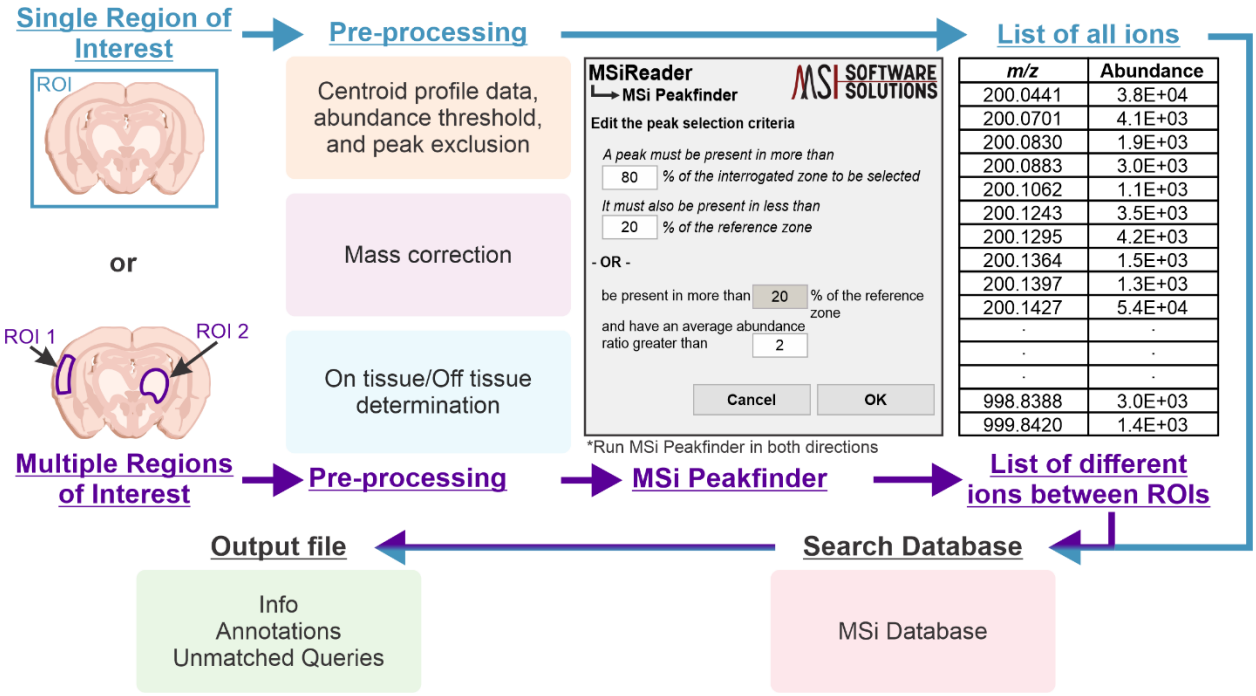

Figure 3.3. MSI data processing workflow for a single (in blue) or for multiple (in purple) ROIs. After obtaining the list of ions, both processes converge to search the database and produce a file of results.

Mass spectrometry data can be natively profile or centroid. Profile data contains multiple data points that form a continuous peak for each *m/z* value. Centroid data, on the other hand, plots discrete values for each *m/z* in the mass spectrum. Nevertheless, MSI data needs to be centroided before analysis in existing software platforms. Therefore, the first tool presented centroids profile data, removes peaks lower than the selected abundance threshold, and has the option to remove ions in a peak exclusion list (*i.e.,* ambient or matrix ions). There are three centroiding algorithms available, parabolic centroid, MSPeaks and local maxima. **Figure 3.4** shows the local maxima and parabolic centroid algorithms. It is recommended to use parabolic centroid for profile data. Local maxima must be selected for data that has already been centroided[18].

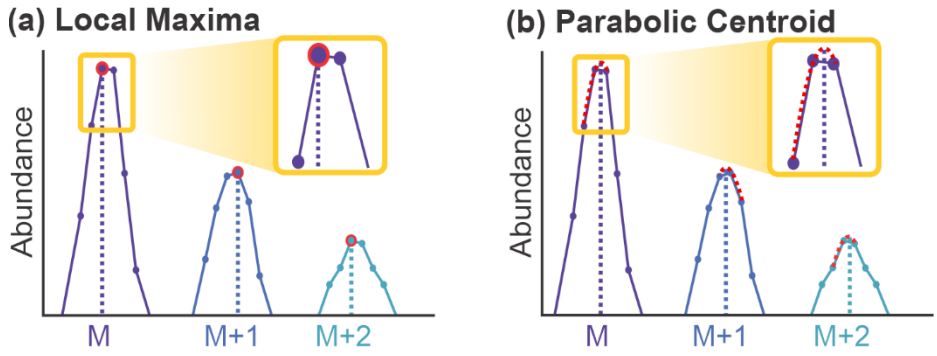

Figure 3.4. Centroiding algorithms. **(a)** Local maxima algorithm takes the highest data point of each peak above the abundance threshold and uses that value as the centroided *m/z* and abundance. **(b)** Parabolic centroid algorithm takes the top three data points, fits a parabola, and takes the apex of the parabola as the *m/z* value and abundance.

Additionally, the mass correction tool allows the user to externally calibrate data. It is needed when the instrument cannot use a lock mass as an internal standard. This happens when the *m/z* range does not include the lock mass (*e.g.,* lock mass *m/z* 200, mass range *m/z* 500-1500). Likewise, some mass spectrometers do not have the capability to select a lock mass for mass correction. Therefore, the user can correct the data externally using an ambient ion, or a highly abundant ion across the whole tissue. Moreover, the Ion Classification Tool (ICT) uses Object-based image analysis (OBIA) to determine if the ions are on tissue or background[19]. This tool uses ion images and can perform batch processing to analyze multiple images at the same time.

To compare multiple ROIs, the user can use MSi Peakfinder. It looks for differences between the interrogated and the reference ROI with the specified conditions. The user should run the tool twice switching the reference and interrogated ROIs to find all the differences. After running the tool, the list of *m/z* and abundance can be used in the searching tool to annotate the data.

To test the functionality of the workflow we used healthy mouse brain data imaged for *N*-linked glycans. This dataset was analyzed as a single ROI, from *m/z* 500-2000 and was natively

profile data. The first step was to centroid the data using the parabolic centroid algorithm with an abundance threshold of 100. Given the mass range, there are no ambient ions present in the mass spectrum. Thus, the peak exclusion filter was not used. The centroided data was then mass corrected using *m/z* 652.1861, which was found to be abundant across the whole tissue. **Figure 3.5(a)** shows the MMA probability histograms for *m/z* 652.1861 from the original and the mass corrected datasets. As shown, the original dataset had a wider trend and the center of the curve is *ca.* 1 ppm. Conversely, the mass corrected data shows the center at 0 ppm and the bins are between -1 and 1 ppm, narrowing the curve.

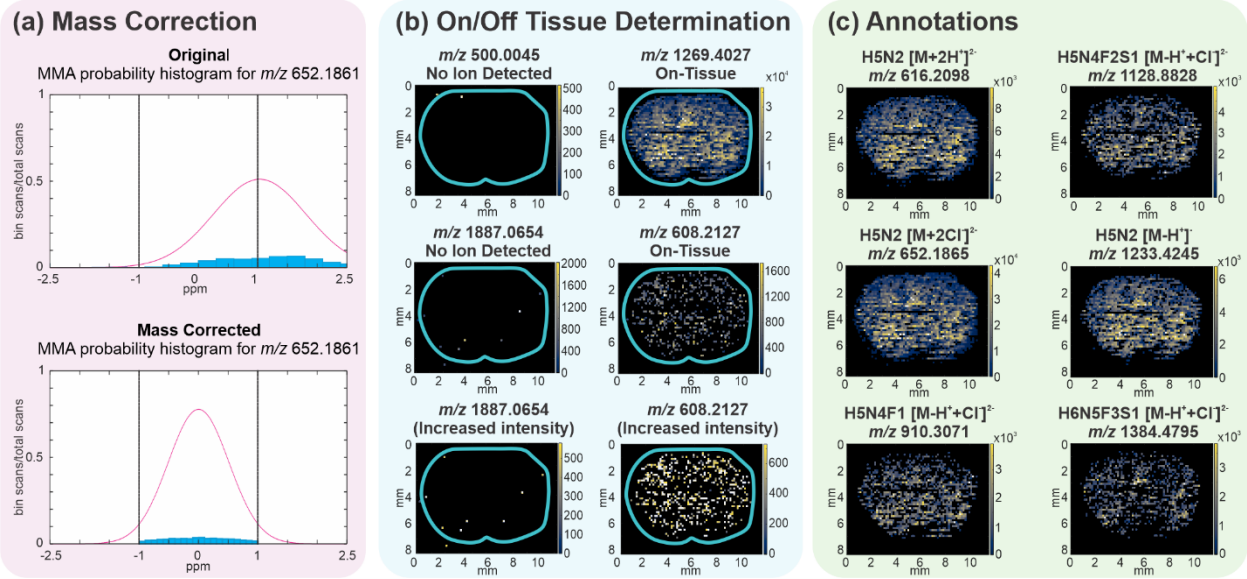

Figure 3.5. Example analyzing healthy mouse brain tissue for *N*-linked glycans. The data was analyzed in a single ROI, with a mass range of *m/z* 500-2000, and collected in profile mode. **(a)** MMA probability histograms for the original and mass corrected datasets. **(b)** Examples of heatmaps with no ion detected and on-tissue ions. The two heatmaps on the bottom have increased intensities that show no background ions. **(c)** Examples of annotations.

The sample prep to analyze *N*-linked glycans removes the lipids and metabolites that may suppress an ion signal. Additionally, since there are no ambient ions in the mass range, the ICT was adjusted to determine “On-tissue” ions and “No ion present”. **Figure 3.5(b)** shows two examples of heatmaps with no ion detected and ions on-tissue. The bottom two heatmaps have an increased intensity to show that there are no background ions present.

After pre-processing the data, we performed the test to annotate ions with the proposed DB. The match tolerance used was 2.5 ppm. **Table 3.2** shows examples of annotations along with **Figure 3.5(c)** which shows nine heatmaps. As shown, most ions are multiply-charged species which would not have been annotated by METASPACE.

Table 3.2. Examples of *N*-linked glycans annotations for healthy mouse brain.

Query m/z	Abundance	Theoretical m/z	MMA (ppm)	Monoisotopic Mass	Molecule Name(s)	Formula	Adduct	Charge State(s)	Molecular class	Sample Type
608.2127	6.4E+02	608.2120	1.14	1218.438512	H4N2F1	C46H78O35N2	$[M-2H^+]^{2-}$	2	*N*-Linked Glycans	Tissue
616.2098	3.1E+03	616.2094	0.57	1234.433427	H5N2	C46H78O36N2	$[M-2H^+]^{2-}$	2	*N*-Linked Glycans	Tissue
634.1974	5.4E+03	634.1978	0.67	1234.433427	H5N2	C46H78O36N2	$[M-H^++Cl^-]^{2-}$	2	*N*-Linked Glycans	Tissue
644.1897	6.4E+02	644.1887	1.67	1218.438512	H4N2F1	C46H78O35N2	$[M+2Cl^-]^{2-}$	2	*N*-Linked Glycans	Tissue
652.1865	1.2E+04	652.1861	0.52	1234.433427	H5N2	C46H78O36N2	$[M+2Cl^-]^{2-}$	2	*N*-Linked Glycans	Tissue
910.3071	1.3E+03	910.3061	1.13	1786.650081	H5N4F1	C68H114O50N4	$[M-H^++Cl^-]^{2-}$	2	*N*-Linked Glycans	Tissue
928.2963	2.3E+03	928.2944	2.00	1786.650081	H5N4F1	C68H114O50N4	$[M+2Cl^-]^{2-}$	2	*N*-Linked Glycans	Tissue
1128.8839	1.6E+03	1128.8828	0.99	2223.803406	H5N4F2S1	C85H141O62N5	$[M-H^++Cl^-]^{2-}$	2	*N*-Linked Glycans	Tissue
1144.8783	9.0E+02	1144.8777	0.51	2255.793235	H6N4F1Gc1	C85H141O64N5	$[M-H^++Cl^-]^{2-}$	2	*N*-Linked Glycans	Tissue
1233.4245	2.4E+03	1233.4262	1.35	1234.433427	H5N2	C46H78O36N2	$[M-H^+]^-$	1	*N*-Linked Glycans	Tissue
1269.4027	1.1E+04	1269.4028	0.09	1234.433427	H5N2	C46H78O36N2	$[M+Cl^-]^-$	1	*N*-Linked Glycans	Tissue
1384.4795	1.2E+03	1384.4778	1.22	2734.993511	H6N5F3S1	C105H174O76N6	$[M-H^++Cl^-]^{2-}$	2	*N*-Linked Glycans	Tissue

This example shows the importance of having an MSI centric DB and a customizable searching tool that accommodates multiply-charged ions. Additionally, a novel scoring system is currently being developed to complement the annotations and provide a level of confidence for the user. The unmatched queries list allows the user to further investigate these ions, and possibly add the new identifications to the DB for future annotations.

3.4 References

(1) Caprioli, R. M. Imaging Mass Spectrometry: Molecular Microscopy for the New Age of Biology and Medicine. *Proteomics* **2016**, *16* (11–12), 1607–1612. https://doi.org/10.1002/pmic.201600133.

(2) Wang, M. F.; Joignant, A. N.; Sohn, A. L.; Garrard, K. P.; Muddiman, D. C. Time of Acquisition and High Spatial Resolution Mass Spectrometry Imaging. *Journal of Mass Spectrometry* **2023**, *58* (3). https://doi.org/10.1002/jms.4911.

(3) Ikegawa, M.; Kakuda, N.; Miyasaka, T.; Toyama, Y.; Nirasawa, T.; Minta, K.; Hanrieder, J. Mass Spectrometry Imaging in Alzheimer's Disease. *Brain Connect* **2023**. https://doi.org/10.1089/brain.2022.0057.

(4) Dekker, J.; Larson, T.; Tzvetkov, J.; Harvey, V. L.; Dowle, A.; Hagan, R.; Genever, P.; Schrader, S.; Soressi, M.; Hendy, J. Spatial Analysis of the Ancient Proteome of Archeological Teeth Using Mass Spectrometry Imaging. *Rapid Communications in Mass Spectrometry* **2023**, *37* (8). https://doi.org/10.1002/rcm.9486.

(5) Ellis, S. R.; Soltwisch, J. Mass Spectrometry Imaging of Lipids. In *Mass Spectrometry for Lipidomics*; Wiley, 2023; pp 117–150. https://doi.org/10.1002/9783527836512.ch5.

(6) Wang, M. F.; Sohn, A. L.; Samal, J.; Erning, K.; Segura, T.; Muddiman, D. C. Lipidomic Analysis of Mouse Brain to Evaluate the Efficacy and Preservation of Different Tissue Preparatory Techniques by IR-MALDESI-MSI. *J Am Soc Mass Spectrom* **2023**, *34* (5), 869–877. https://doi.org/10.1021/jasms.2c00353.

(7) Mellinger, A. L.; Muddiman, D. C.; Gamcsik, M. P. Highlighting Functional Mass Spectrometry Imaging Methods in Bioanalysis. *J Proteome Res* **2022**, *21* (8), 1800–1807. https://doi.org/10.1021/acs.jproteome.2c00220.

(8) Sohn, A. L.; Ping, L.; Glass, J. D.; Seyfried, N. T.; Hector, E. C.; Muddiman, D. C. Interrogating the Metabolomic Profile of Amyotrophic Lateral Sclerosis in the Post-Mortem Human Brain by Infrared Matrix-Assisted Laser Desorption Electrospray Ionization (IR-MALDESI) Mass Spectrometry Imaging (MSI). *Metabolites* **2022**, *12* (11), 1096. https://doi.org/10.3390/metabo12111096.

(9) Pace, C. L.; Angel, P. M.; Drake, R. R.; Muddiman, D. C. Mass Spectrometry Imaging of *N* -Linked Glycans in a Formalin-Fixed Paraffin-Embedded Human Prostate by Infrared Matrix-Assisted Laser Desorption Electrospray Ionization. *J Proteome Res* **2022**, *21* (1), 243–249. https://doi.org/10.1021/acs.jproteome.1c00822.

(10) Müller, W. H.; Verdin, A.; De Pauw, E.; Malherbe, C.; Eppe, G. Surface-assisted Laser Desorption/Ionization Mass Spectrometry Imaging: A Review. *Mass Spectrom Rev* **2022**, *41* (3), 373–420. https://doi.org/10.1002/mas.21670.

(11) Gao, S.; Zhao, J.; Guan, Y.; Tang, Y.; Li, Y.; Liu, L. Mass Spectrometry Imaging Technology in Metabolomics: A Systematic Review. *Biomedical Chromatography* **2022**. https://doi.org/10.1002/bmc.5494.

(12) Feucherolles, M.; Frache, G. MALDI Mass Spectrometry Imaging: A Potential Game-Changer in a Modern Microbiology. *Cells* **2022**, *11* (23), 3900. https://doi.org/10.3390/cells11233900.

(13) Caleb Bagley, M.; Garrard, K. P.; Muddiman, D. C. The Development and Application of Matrix Assisted Laser Desorption Electrospray Ionization: The Teenage Years. *Mass Spectrom Rev* **2021**, mas.21696. https://doi.org/10.1002/mas.21696.

(14) Baquer, G.; Sementé, L.; Mahamdi, T.; Correig, X.; Ràfols, P.; García-Altares, M. What Are We Imaging? Software Tools and Experimental Strategies for Annotation and Identification of Small Molecules in Mass Spectrometry Imaging. *Mass Spectrom Rev* **2022**. https://doi.org/10.1002/mas.21794.

(15) Bokhart, M. T.; Nazari, M.; Garrard, K. P.; Muddiman, D. C. MSiReader v1.0: Evolving Open-Source Mass Spectrometry Imaging Software for Targeted and Untargeted Analyses. *J Am Soc Mass Spectrom* **2018**, *29* (1), 8–16. https://doi.org/10.1007/s13361-017-1809-6.

(16) Robichaud, G.; Garrard, K. P.; Barry, J. A.; Muddiman, D. C. MSiReader: An Open-Source Interface to View and Analyze High Resolving Power MS Imaging Files on Matlab Platform. *J Am Soc Mass Spectrom* **2013**, *24* (5), 718–721. https://doi.org/10.1007/s13361-013-0607-z.

(17) Palmer, A.; Phapale, P.; Chernyavsky, I.; Lavigne, R.; Fay, D.; Tarasov, A.; Kovalev, V.; Fuchser, J.; Nikolenko, S.; Pineau, C.; Becker, M.; Alexandrov, T. FDR-Controlled Metabolite Annotation for High-Resolution Imaging Mass Spectrometry. *Nat Methods* **2017**, *14* (1), 57–60. https://doi.org/10.1038/nmeth.4072.

(18) Kibbe, R. R.; Muddiman, D. C. Achieving Sub-Parts-per-Million Mass Measurement Accuracy on an Orbitrap Mass Spectrometry Imaging Platform without Automatic Gain Control. *J Am Soc Mass Spectrom* **2023**. https://doi.org/10.1021/jasms.3c00004.

(19) Eisenberg, S. M.; Knizner, K. T.; Muddiman, D. C. Development of an Object-Based Image Analysis Tool for Mass Spectrometry Imaging Ion Classification. *Anal Bioanal Chem* **2023**. https://doi.org/10.1007/s00216-023-04764-x.

APPENDICES

A1. Supplemental Information for Chapter 2

Table A.3. Parts used to construct the IR-MALDESI source

IR-MALDESI	**Item**	**Vendor**	**Prod#**	**Quant**	**Description**	**Link**
Structure	Silver breadboard 18" x 18" x0.5" 1/4-20 (Base)	Newport	SA2-18X18-LC	1	Optical breadboard plate 18 x 18 x 0.5in. Solid Aluminum, LaserClean	https://www.newport.com/p/SA2-18x18-LC
	Silver breadboard 18" x 12" x0.5" 1/4-20 (Upper)	Thorlabs	MB1218U	1	Unanodized Aluminum Breadboard, 12" x 18" x 1/2", 1/4"-20 Taps	https://www.thorlabs.com/thorproduct.cfm?partnumber=MB1218U
	T-Slotted Framing Single, 4*24"	McMaster-Carr	47065T801	4	Silver Anodized Aluminum $0.62/inch	https://www.mcmaster.com/rails/t-slotted-framing-rails/
	Small corner bracket	McMaster-Carr	2313N793	8	Sets of 2. Corner machine bracket with 2 mounting slots, 6061 Al, 1-1/2" x 1" x 1"	https://www.mcmaster.com/catalog/127/2773/
	Large corner bracket	McMaster-Carr	2313N794	8	Corner machine bracket with 2 mounting slots, 6061 Al, 2" x 1" x 1". Unit	https://www.mcmaster.com/catalog/127/2773
	T-nuts for McMaster-Carr construction rails	McMaster-Carr	98001A130	1	Pack of 25. Low-profile narrow-base weld nut, 1/4"-20 thread size, 1" long	https://www.mcmaster.com/tee-nuts/low-profile-narrow-base-weld-nuts-8/
	Screws 1/4"-20 for assembling	Thorlabs	SH25S075	3	Pack of 25. 1/4"-20 Stainless steel cap screw, 3/4" long	https://www.thorlabs.com/thorproduct.cfm?partnumber=SH25S075
Stages	XY stage	Newport	ONE-XY100	1	Motorized XY Linear Stage, Linear Motor, 90mm Travel	https://www.newport.com/p/ONE-XY100
	Z stage	Newport	GTS30V	1	High Precision Vertical Stage, 30mm Travel	https://www.newport.com/p/GTS30V
	Motion Controller	Newport	XPS-RLD4	1	Motion Controller, 4-axis Universal Driver, Ethernet, Basic GPIO and PCO	https://www.newport.com/p/XPS-RLD4
	Linear drive module	Newport	XPS-DRV02	2	Linear drive module for brushless motors, 5A/44Vpp max	https://www.newport.com/p/XPS-DRV02

	Encoder adapter	Newport	E5820A	2	Encoder adapter, XPS-D, DB15 to HD26, For ILS-LM-S, VP-25XL	https://www.newport.com/p/E5820A
	Universal digital driver	Newport	XPS-DRV11	1	Universal digital driver card for Stepper, DC, Brushless and Direct	https://www.newport.com/p/XPS-DRV11
	Interface plate between axis	McMaster-Carr	3511T34	1	Tight-Tolerance Multipurpose 6061 Aluminum with Certificate, Precision Ground on Top and Bottom, 12" x 18", 1/2" Thick. This piece is cut and drilled the holes to fit the XY stage	https://www.mcmaster.com/3511T34/
	Sample stage	McMaster-Carr	9246K464	1	Multipurpose 6061 Aluminum, 5/16" Thick, 6" x 12"	https://www.mcmaster.com/9246K464/
	Screws for sample stage to Z-axis	McMaster-Carr	94500A236	1	316 Stainless steel button head hex drive screws M6 x 1mm thread x 12mm long. Pack of 50	https://www.mcmaster.com/94500A236/
	Screws for Z-axis to interface plate	McMaster-Carr	94500A238	1	316 Stainless steel button head hex drive screws M6 x 1mm thread x 20mm long. Pack of 25	https://www.mcmaster.com/94500A238/
	Washer for Z-axis to interface plate	McMaster-Carr	98689A115	1	General purpose 18-8 stainless steel washer fro M6 screws, 6.4mm ID, 11mm OD. Pack of 100	https://www.mcmaster.com/98689A115/
	Screws for interface plate to XY stage	McMaster-Carr	94500A233	1	316 Stainless steel button head hex drive screws M5 x 0.8 thread x 20mm long. Pack of 50	https://www.mcmaster.com/94500A233/
Peltier cooled stage	Garolite	McMaster-Carr	8667K118	1	Flame-retardant garolite G-10/FR4 sheet	https://www.mcmaster.com/8667K118/
	Waterblock	Custom Thermoelectric	WBAC-0750-0750-012.7-CU-NCSU	1	Water block liquid heat exchanger	Custom order
	Neoprene	McMaster-Carr	1601N213	1	Multipurpose neoprene foam	https://www.mcmaster.com/1601N213/
	Peltier cooler	TE Tech	TE-195-1.0-0.8	1	Peltier Cooler (potted) w/ thermal paste	https://tetech.com/product/te-195-1-0-0-8/
	Sample holder	McMaster-Carr	89015K163	1	Multipurpose 6061 Aluminum sheet, 0.04" thick, 6" x 6"	https://www.mcmaster.com/89015K163/
	Thermal paste	TE Tech	TP-1	1	General purpose zinc oxide termal paste that improves heat transfer betwwen adjoining surfaces	https://tetech.com/product/tp-1/

	Koolance water cooler	Koolance	EX2-755	1	EX2-755 Computer liquid cooling system	https://koolance.com/ex2-755-exos-2-v2-liquid-cooling-system-aluminum
	AC adaptor for Koolance water cooler	Koolance	ADT-EX004S	1	AC Power adapter for EXT/EX2 systems	https://koolance.com/exos-ac-power-adapter
	Koolance hose fitting	Koolance	NZL-V13BS	2	Swivel/Lock Barb Fitting fro ID 13mm (1/2in), G1/4 BSSP	https://koolance.com/nozzle-single-swivel-lock-barb-for-id-13mm-1-2in
	Water tubing hose	McMaster-Carr	5233K84	25	Cost per ft. Clear masterkleer soft PVC tubing. 12" ID, 13/16" OD	https://www.mcmaster.com/5233K84/
	Hose clamps	McMaster-Carr	5011T171	1	Worm-drive clamp for firm hose and tube 1/2" - 29/32" clamp ID. Pack of 10	https://www.mcmaster.com/5011T171/
	T-fittings	McMaster-Carr	48315K61	2	High-Pressure plastic pipe fitting for water, tee conector, 1/2 barbed male	https://www.mcmaster.com/48315K61/
	Ball valves	McMaster-Carr	4757K19	2	Dark gray PVC on/off valve barbed fittings for 1/2" tube ID	https://www.mcmaster.com/4757K19/
	DC variable power supply	Amazon	K3010D 4-Digit LED Display	1	Longwei DC power supply variable 30V 10A	https://www.amazon.com/gp/product/B07M9N73YQ/ref=ppx_yo_dt_b_asin_title_o00_s00?ie=UTF8&psc=1
ESI emitter	Construction rail for Z direction	Thorlabs	XE25L12	1	25mm square construction rail. 12" long, 1/4"-20 taps	https://www.thorlabs.com/thorproduct.cfm?partnumber=XE25L12
	Rail for X direction	Thorlabs	RLA03000	1	Dovetail optical rail, 3", imperial	https://www.thorlabs.com/thorproduct.cfm?partnumber=RLA0300
	Rail for Y direction	Thorlabs	RLA06000	1	Dovetail optical rail, 6", imperial	https://www.thorlabs.com/thorproduct.cfm?partnumber=RLA0600
	Rail carrier	Thorlabs	RC1	2	Dovetail rail carrier, 1.00" x 1.00", 1/4" (M6) Counterbored	https://www.thorlabs.com/thorproduct.cfm?partnumber=RC1
Camera	Horizontal rail	Thorlabs	RLA03000	1	Dovetail optical rail, 3", imperial	https://www.thorlabs.com/thorproduct.cfm?partnumber=RLA0300

	Vertical rail	Thorlabs	RLA06000	1	Dovetail optical rail, 6", imperial	https://www.thorlabs.com/thorproduct.cfm?partnumber=RLA0600
	Rail carrier	Thorlabs	RC1	2	Dovetail rail carrier, 1.00" x 1.00", 1/4" (M6) Counterbored	https://www.thorlabs.com/thorproduct.cfm?partnumber=RC1
	Construction cube to connect both dovetail rails	Thorlabs	RM1F	1	1" Construction cube with 1/4" - 20 tapped holes	https://www.thorlabs.com/thorproduct.cfm?partnumber=RM1F#ad-image-0
	Construction rail	McMaster-Carr	47065T807	3	T-slotted framing, single four slot rail, black, 1" high X 1" wide, solid. 3" long. Sold per inch	https://www.mcmaster.com/47065T807/
	Large corner bracket	McMaster-Carr	2313N794	1	Corner machine bracket with 2 mounting slots, 6061 Al, 2" x 1" x 1". Unit	https://www.mcmaster.com/catalog/127/2773
	Focal lens for camera	Edmund	#63-780	1	25mm, 200-600mm primary WD, HP series fixed foacl length lens	https://www.edmundoptics.com/p/25mm-200-600mm-primary-wd-hp-series-fixed-focal-length-lens/18494/
	Camera	FLIR	FL3-U3-120S3C-C	1	FL3-U3-120S3C-C: 12MP, color, 15 FPS, Sony IMX172	https://www.flir.com/products/flea3-usb3/
	Cable	FLIR	ACC-01-2301	1	ACC-01-2301: USB 3.1, 5m, Type-A to Micro-B (Locking) Cable	https://www.flir.com/products/usb-3.1-locking-cable/
	Tripod adapter	FLIR	ACC-01-0003	1	ACC-01-0003: 26.9mm by 17.9mm,1/4"-20 Tripod Adapter	https://www.flir.com/products/tripod-adapter-for-bfs-30mm-bfly-cmln-cm3-ffmv-fl2-fl3-fmvu/
Laser	L-bracket with Fan	JGMA		1		Custom order
	2970 nm laser	JGMA	MSI-0-2970	1		Custom order
	Down tube	JGMA	SM1		Lens tubes. Different heights and models used.	Ø1" Lens Tubes (thorlabs.com)
	Focus lens	Thorlabs	LA6002	1	D=25.4 F=50.0MgF22222 Plano Convex Lens	https://www.thorlabs.com/thorproduct.cfm?partnumber=LA6002
	Beam expander	Thorlabs	LC5401	1	CaF2 Plano-Concave Lens, f = -75.0 mm, Uncoated	Thorlabs - LC5401 Ø1" CaF₂ Plano-

						Concave Lens, f = -75.0 mm, Uncoated
	Telescopic lens holder	Thorlabs	SM1NR1	1	SM1 Zoom housing for ⌀1" optics, non-rotating, 2" (50.8 mm) travel	https://www.thorlabs.com/thorproduct.cfm?partnumber=SM1NR1
	DC variable power supply	Amazon	K3010D 4-Digit LED Display	1	Longwei DC power supply variable 30V 10A	https://www.amazon.com/gp/product/B07M9N73YQ/ref=ppx_yo_dt_b_asin_title_o00_s00?ie=UTF8&psc=1
	AC/DC power supply for fan	Newark	WSU090-0800-13	1	TRIAD AC/DC power supply, 1 output, 9V, 800mA	https://www.newark.com/triad-magnetics/wsu090-0800-13/wall-mount-adaptor-ac-dc-9v-0/dp/05AC7671?ost=WSU090-0800-13&krypto=BsicfOpFq1k35YsnskeHc08hLo344bsyB9g%2Fh%2Br7wYHHwFmJAtCuRyNGpKcwriYwC9z3N8tNMlne821ekuZENPOl8MDV9UArGDo%2B23rLjQnXjCbgFXQobSif4M2fo31%2B
Metal capillary extension	304/304L Stainless Steel Rod	McMaster-Carr	9210K294	1	Easy-to-Machine Multipurpose 304/304L Stainless Steel Rod	https://www.mcmaster.com/9210K29/